SKB

TECHNICAL REPORT 96-20

On the characterization of retention mechanisms in rock fractures

Jan-Olof Selroos, Vladimir Cvetkovic

Division of Water Resources Engineering,
Department of Civil and Environmental Engineering,
Royal Institute of Technology, Stockholm, Sweden

December 1996

SVENSK KÄRNBRÄNSLEHANTERING AB
SWEDISH NUCLEAR FUEL AND WASTE MANAGEMENT CO
P.O.BOX 5864 S-102 40 STOCKHOLM SWEDEN
PHONE +46 8 665 28 00
FAX +46 8 661 57 19

ON THE CHARACTERIZATION OF RETENTION MECHANISMS IN ROCK FRACTURES

Jan-Olof Selroos, Vladimir Cvetkovic

**Division of Water Resources Engineering,
Department of Civil and Environmental Engineering,
Royal Institute of Technology, Stockholm, Sweden**

December 1996

On the Characterization of Retention Mechanisms in Rock Fractures

Jan-Olof Selroos and Vladimir Cvetkovic

Division of Water Resources Engineering
Department of Civil and Environmental Engineering
Royal Institute of Technology
S-100 44 Stockholm, Sweden

December, 1996

Keywords: Rock fractures, aperture variability, matrix diffusion, matrix and surface sorption, tracer transport, prediction uncertainty.

Abstract

Following a hypothetical leakage from a deep-rock nuclear waste repository, radionuclides may migrate through the geosphere to the biosphere. Since most nuclides are retarded during the migration process, the geosphere is considered part of the multi-barrier system. Hence it is of interest to understand the relevant retention processes in the fractured rock of the geosphere.

Radionuclide transport in fractured media is controlled by advection and mass transfer processes. Advection primarily takes place along single fractures, whereas mass transfer such as surface sorption and matrix diffusion occurs at the fracture surfaces. Aperture heterogeneity thus affects both advection and mass transfer characteristics. This spatial heterogeneity, in combination with sparse aperture measurements, results in a prediction uncertainty with implications for both fracture characterization in the field and for safety assessment applications.

An analytical solution for the mass flux in a single fracture is derived using the stochastic Lagrangian travel time approach. Combined matrix diffusion and equilibrium sorption (matrix and surface) are incorporated in the analysis. The solution is dependent on three variables: the conservative solute travel time, τ, a parameter accounting for solute characteristics, κ, and a parameter related to the fluid discharge and surface available for diffusion and sorption, β. Based on the analytical mass flux solution and underlying moments of β and τ, the first two mass flux moments and first two moments of the time for a given accumulated mass fraction are derived.

The results are illustrated for a kinematic flow path with pre-defined aperture and width statistics. The moments of β and τ are derived analytically for the simplified flow case. The effect of variability and spatial correlation structure of aperture and width on the mass flux moments and moments of the time for a given accumulated mass fraction are investigated. The implications of the results for field-scale tracer test (characterization) and for safety assessment applications are discussed. The possible correlation between travel time, τ, and parameter β for increasingly complex flow conditions and/or evolving scales is identified as a key issue in both applications.

Sammanfattning

Radionuklider kan transporteras genom geosfären till biosfären efter ett hypotetiskt läckage i ett djupförvar för radioaktivt avfall. Geosfären betraktas som en del av flerbarriärssystemet eftersom de flesta nuklider utsätts för retention under transporten. Sålunda är det av intresse att öka förståelsen för de relevanta retentionsmekanismerna i geosfärens sprickiga berg.

Transport av radionuklider i ett sprickigt medium styrs av advektion och massöverföringsprocesser. Advektion sker huvudsakligen längs med enskilda sprickor, medan massöverföringsprocesser såsom ytsorption och matrisdiffusion sker vid sprickytorna. En heterogenitet i sprickapertur kommer sålunda att påverka både advektions- och massöverföringskarakteristik. Denna rumsliga variabilitet kombinerad med få mätningar resulterar i en prediktionsosäkerhet som får konsekvenser för både sprick-karakterisering i fält samt för olika tillämpningar inom säkerhetsanalys.

En analytisk lösning för massflödet i en enskild spricka härleds med hjälp av en stokastisk-lagrangisk analys för transporttider. Analysen inkorporerar kombinerad matrisdiffusion och jämviktssorption (matris- och ytsorption). Lösningen beror på tre variabler: den konservativa transporttiden, τ, en parameter som beror på det transporterade ämnets egenskaper, κ, samt på en parameter som kan relateras till flöde och tillgänglig yta för diffusion och sorption, β. De två första statistiska momenten för massflödet samt för tiden att uppnå en given kumulativ massfraktion härleds och baseras på den analytiska massflödeslösningen samt på de underliggande statistiska momenten av β och τ.

Resultaten illustreras för en kinematisk flödesbana med fördefinierad statistik för apertur och flödesbredd. De statistiska momenten för β och τ härleds analytiskt för detta förenklade flödesfall. De resulterande massflödes- och tidsmomentens beroende på korrelationsstruktur samt på rumslig variabilitet i apertur och flödesbanans bredd undersöks. Vidare diskuteras resultatens konsekvenser för fältskaliga spårämnesförsök (karakterisering) samt för säkerhetsanalys. Under allt mer komplexa flödesförhållanden och/eller ökande rumsskalor identifieras en eventuell korrelation mellan transporttiden, τ, och parametern β som en central fråga i de två tillämpningarna.

Contents

1 Background

The controlling mechanisms of radionuclide migration in fractured media are advection by groundwater and exchange of radionuclide mass with the rock matrix. The advection is believed to take place primarily along fractures, whereas the mass transfer occurs from the mobile water in the fractures to the stagnant water of the rock matrix by diffusion and sorption. Matrix diffusion is potentially an important process in the retention of radionuclides escaping from a repository for nuclear waste in the bedrock (e.g., *Neretnieks*, 1980; *Abelin*, 1985; *Frick et al.*, 1992; *Neretnieks*, 1993; *Olsson et al.*, 1995). Recently a comprehensive experimental program has been initiated at the SKB Äspö Hard Rock Laboratory, focused on evaluating tracer retention mechanisms on different scales (*Winberg*, 1994).

In spite of the effort over the past few decades to understand tracer retention in fractured rock, a number of open questions still remain. One important unresolved issue is how the flow path geometry, specifically the surface area available for sorption, influences matrix diffusion as well as surface sorption (e.g., *Moreno and Neretnieks*, 1993, *Moreno et al.*, 1995) and how it can be characterized in the field (e.g., *Olsson et al.*, 1995). A related question is how to assess the prediction uncertainty resulting from the natural variability in flow path geometry.

Most of the currently available analytical models of transport in fractures that account for matrix diffusion are based on flow paths defined as uniform rectangular channels (e.g. *Moreno and Neretnieks*, 1993). Analytical models that account for the variability in fracture transmissivity also assume uniform fracture aperture for diffusion (*Cvetkovic*, 1991). Numerical models for tracer transport in fractures with variable aperture that account for matrix diffusion and sorption are available (e.g. *Moreno et al.* (1995) based on *Moreno et al.* (1988)).

In this study we propose a theoretical framework that incorporates matrix diffusion combined with equilibrium sorption within the Lagrangian travel (residence) time approach. We define a kinematic prototype of a *flow path* that is believed to capture the essential features: spatial variability of the aperture and width, and derive an analytical model for coupled tracer advection and mass transfer for transport in fractures. The considered flow path model is consistent with the ideas presented by O. Olsson in *Olsson et al.* (1995). The theoretical results presented in this report generalize the result of *Cvetkovic* (1991). Also, the results of this report can be shown to be a particular case within a more general framework proposed by *Cvetkovic and Dagan* (in preparation)

where the Lagrangian approach to coupled advection-reaction processes in heterogeneous formations (*Cvetkovic and Dagan*, 1994, 1996; *Dagan and Cvetkovic*, 1996) has been extended to account for the heterogeneity in reaction parameters.

Due to flow path heterogeneity, the residence time will be random, and the parameter governing matrix diffusion and sorption will also be random. Analytical expressions for the resulting mass flux moments are derived in terms of these random parameters. In the illustration examples, the effect of hypothetical (generic) flow path geometries is investigated. A simple expression is derived for estimating the mean and variance of the arrival time of a given radionuclide mass fraction, from a repository to the biosphere. We also discuss the type of modelling studies that combined with field and laboratory experiments can contribute towards more accurate characterization of retention mechanisms in the field.

2 Problem formulation and scope

2.1 Retention of radionuclides and safety assessment

We consider a hypothetical radionuclide release from a canister at A, and at time t_0 after the closure of a repository (Figure 2.1). The release can be a pulse or continuous; for illustrative purposes we shall consider a pulse. The radionuclide is advected by groundwater along a flow path from A to B, where B is the point of radionuclide discharge into the biosphere (Figure 2.1). Since the size of the release location A is anticipated *small* in comparison to the scale of the transport problem (i.e., distance AB), we neglect the dispersion due to flow heterogeneity *within* the flow path AB. Thus if the radionuclide is not subject to mass transfer (i.e., retention) or decay, the pulse would arrive at B intact; however, its time of arrival, τ, would be *uncertain* due to flow heterogeneity. The corresponding cumulative mass arrival would be a step function i.e., all released mass would arrive at time τ, that coincides with the groundwater residence time between AB, counted from the release time t_0 (Figures 2.2a and 2.2b, case $\kappa^* = 0$).

In the general case, a radionuclide released at A is subject to physical mass transfer (diffusion) and sorption, as well as to decay, as it is advected by groundwater toward the discharge point B. To make the effects of retention more apparent, we neglect decay. The qualitative effect of diffusion and sorption is illustrated in Figure 2.2, where the parameter κ^* is proportional both to the rate of diffusion and sorption in the matrix; $\kappa^* = 0$ implies conservative transport, i.e. pure advection. For high κ^*, the dose of the radionuclide discharge into the biosphere at B, may be significantly reduced, and also shifted in time allowing for more substantial decay. If sufficiently strong, the retention processes may radically transform the discharge of radionuclides into the biosphere, as compared to conservative (nonreactive) advective transport. In the safety assessment context, it is therefore critical to provide a realistic evaluation of the possible retention likely to take place in the bedrock.

2.2 The general configuration

We consider a host rock formation where groundwater flow takes place along conducting fractures. For simplicity, the fractures are conceptualized as essentially two-dimensional features. The advection flow path from the canister A to the biosphere B, is assumed to take place along a path possibly connecting many single fractures, thus forming a three-dimensional network (Figure 2.3). It is convenient to focus our following analysis on a single fracture, although the results are applicable to the entire network; this will

be discussed subsequently.

2.3 Kinematic prototype of a flow path in a fracture

In a two-dimensional fracture plane, flow paths which are dependent on the scale of the release point A are obtained from streamlines. In Figure 2.4 one such flow path within a fracture plane is indicated by thick marking of two adjacent streamlines, obtained by solving the 2D flow equation with spatially variable transmissivity. Thus the actual advection flow paths in fractures are artifacts of the flow dynamics, including the heterogeneous aperture distribution and the flow and mass injection boundary conditions. In the present investigation, we shall make a major simplification and *neglect* the flow dynamics. The basic configuration to be adopted in the following is a generalization of the kinematic flow path proposed by O. Olsson (*Olsson et al.*, 1995) (Figure 2.5). The use of the kinematic flow path is consistent with the current understanding of solute transport in fractures. It is generally hypothesized that flow in fracture planes occur in well-defined channels such as the one proposed here.

Consider a hypothetical flow path in a fracture shown in Figure 2.6a. For a given fluid discharge Q, the fluid velocity is a random space function (RSF) due to the variability in the cross-sectional area. We shall assume this area to be rectangular, defined as a product of a width (w) and an aperture ($2b$), both of which are RSFs and defined as functions of x_1.

Although a flow path may meander arbitrarily within a fracture plane, this fact is irrelevant in the present context. In particular, the relevant flow path cross-sectional area is the one orthogonal to the mean flow, since it determines the fluid (and tracer) residence time across the fracture. Thus we define the kinematic prototype of a flow path in 1D, with varying width and aperture along x_1, that can in effect represent an infinite number of 2D flow paths with the same width $w(x_1)$ and half-aperture $b(x_1)$; in Figure 2.6b a sketch of two possible (meandering) realizations from the same single (straight) flow path prototype, is presented. The flow path is "sliced" by elementary surfaces that are orthogonal to the mean flow, with elementary volumes evaluated as $dA\,dx_1$ where $dA = 2bw$ (Figure 2.7a and 2.7b).

2.4 Scope

The objective of this report is to use the simplified kinematic representation of a flow path (Figures 2.6-2.7) and to analyze the impact of flow path geometry on the tracer

retention in fractures. We shall consider a relatively wide range of correlation structures for w and b, and show how these affect tracer retention. We identify a key parameter for mass transfer, and discuss its significance for field-scale characterization, as well as for safety assessment. Even though the presented theory is developed based on the kinematic prototype of a flow path, most of the results are general and applicable to transport in a two-dimensional fracture with spatially variable aperture. This point will be discussed in Section 7.

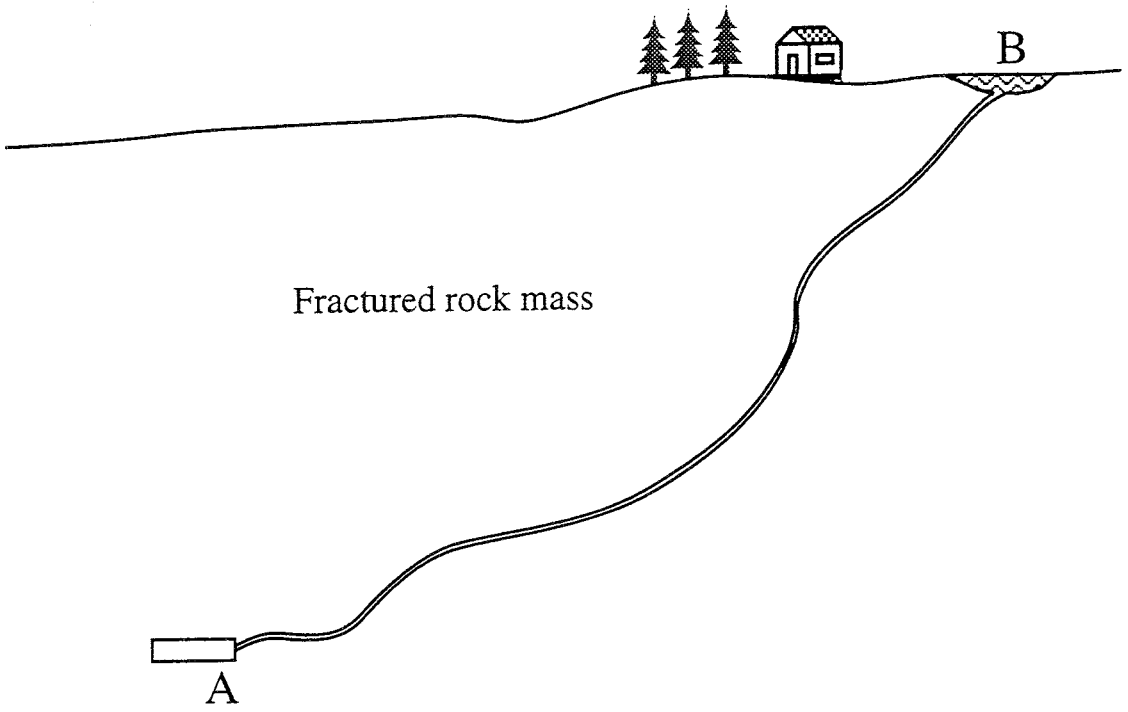

Figure 2.1 *Single flow path from radionuclide release point A to point of discharge into the biosphere B.*

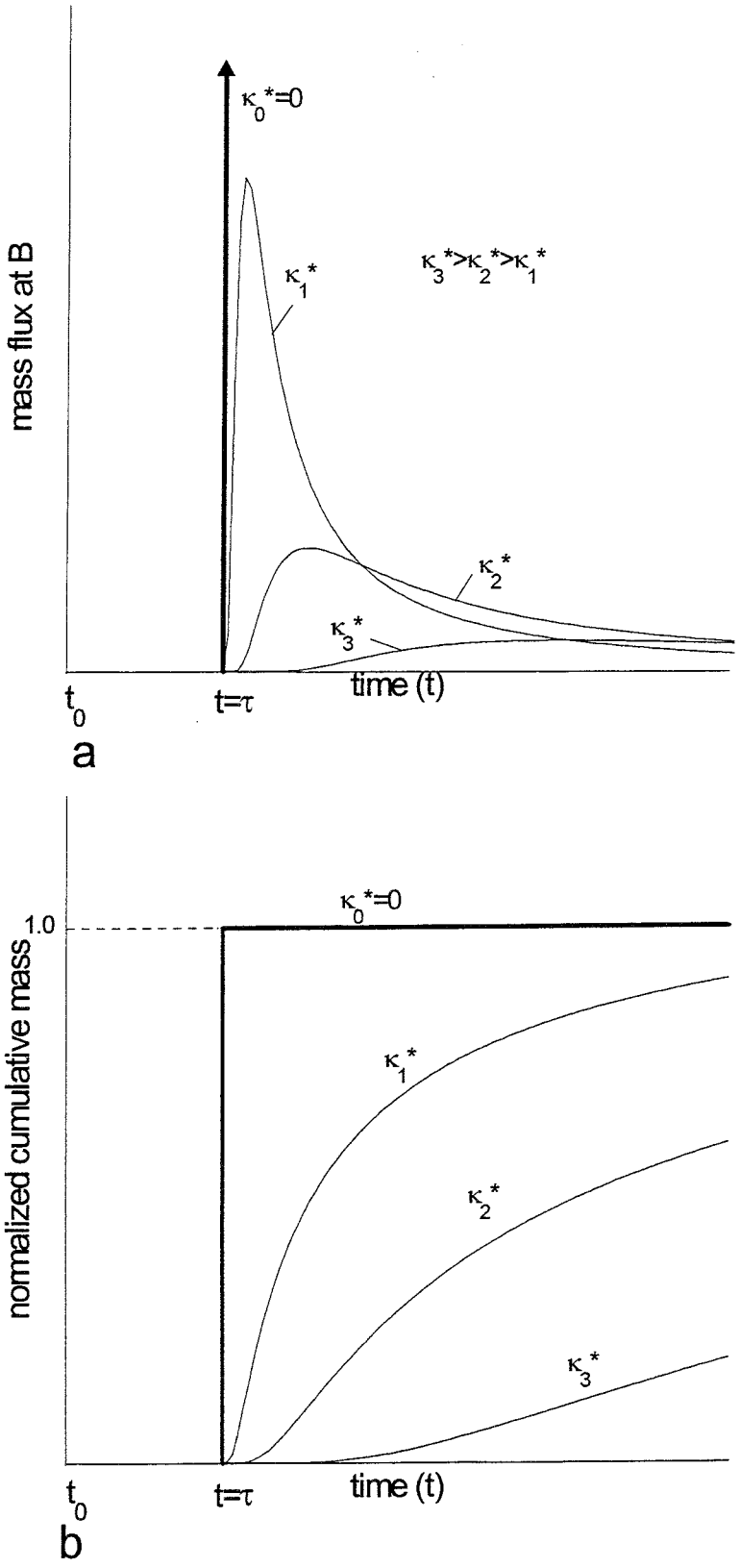

Figure 2.2 *Mass flux (a) and cumulative mass arrival (b) at B for a conservative radionuclide ($\kappa^* = 0$) and for reactive radionuclides with $\kappa_3^* > \kappa_2^* > \kappa_1^*$.*

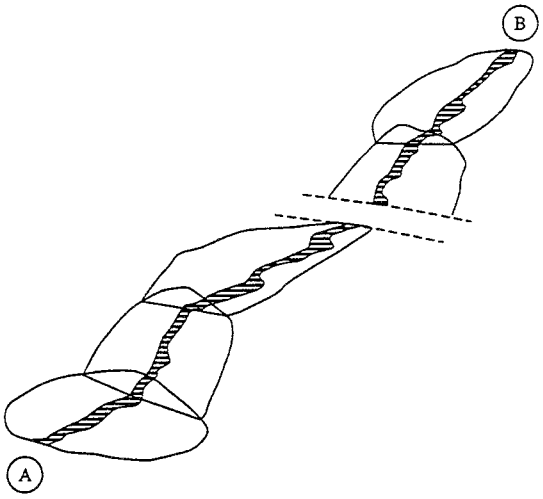

Figure 2.3 *Single flow path meandering through several individual fracture planes on its way from release point A to discharge point B.*

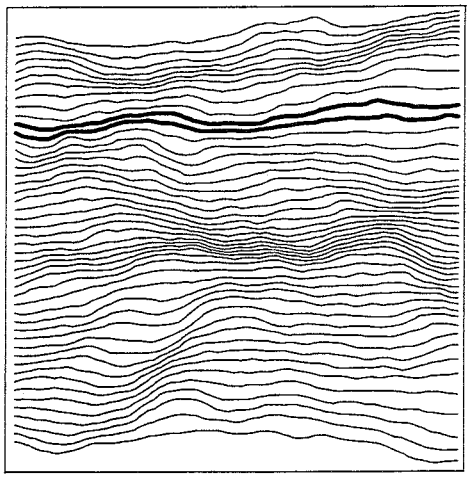

Figure 2.4 *Streamlines and a single flow path in a two-dimensional fracture plane.*

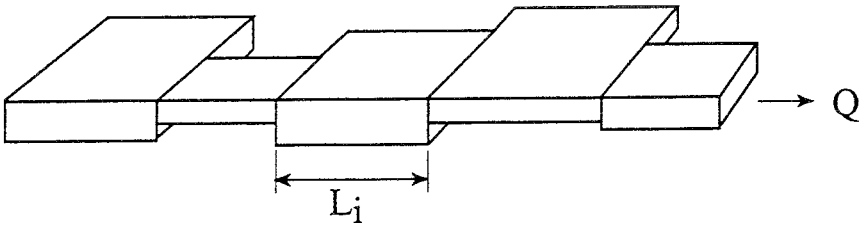

Figure 2.5 *Kinematic flow path with discretely varying aperture and width.*

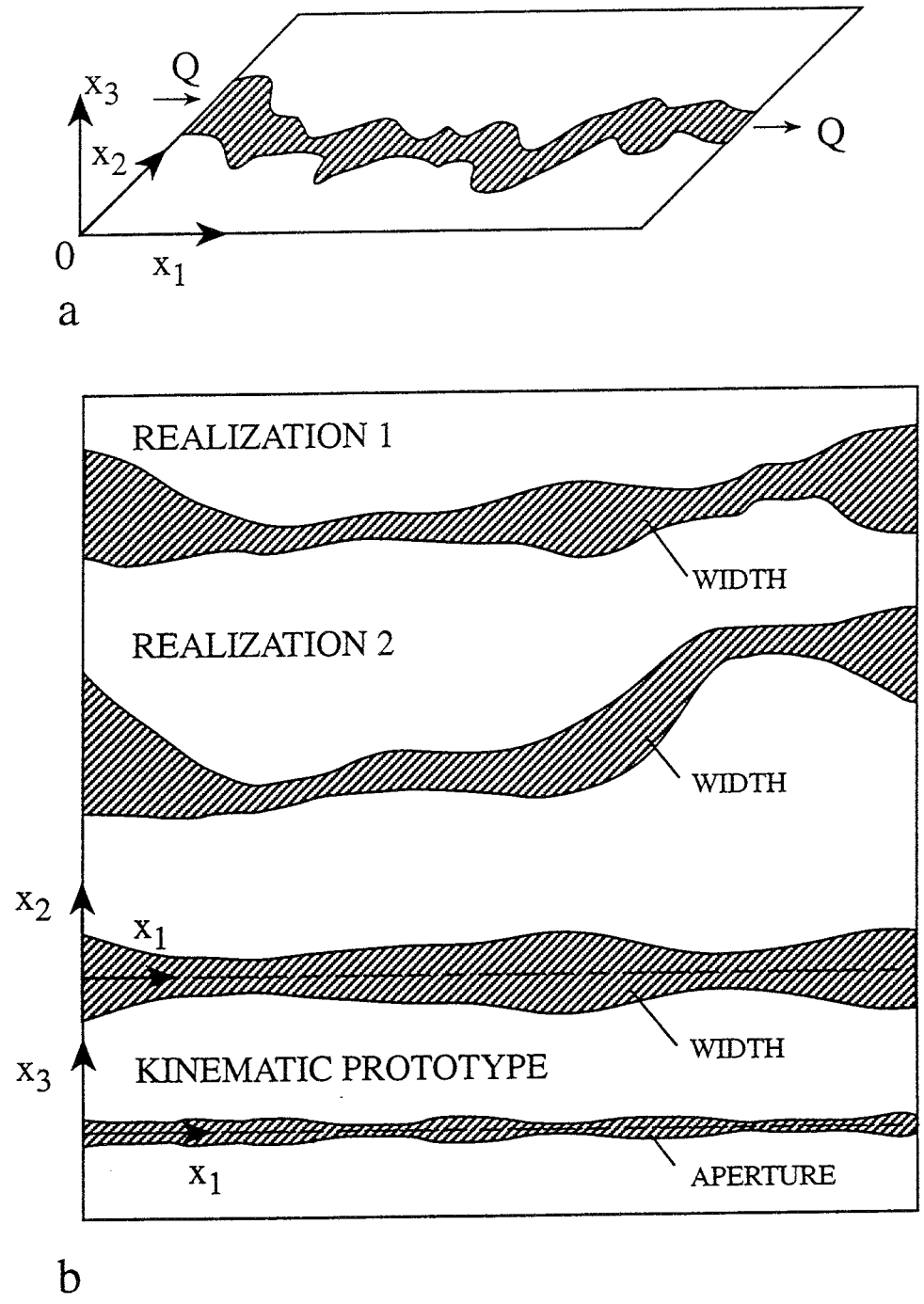

Figure 2.6 *a) Hypothetical flow path in a fracture. b) Two flow path realizations with meandering shape, and resulting prototype flow path representing each of the meandering flow paths.*

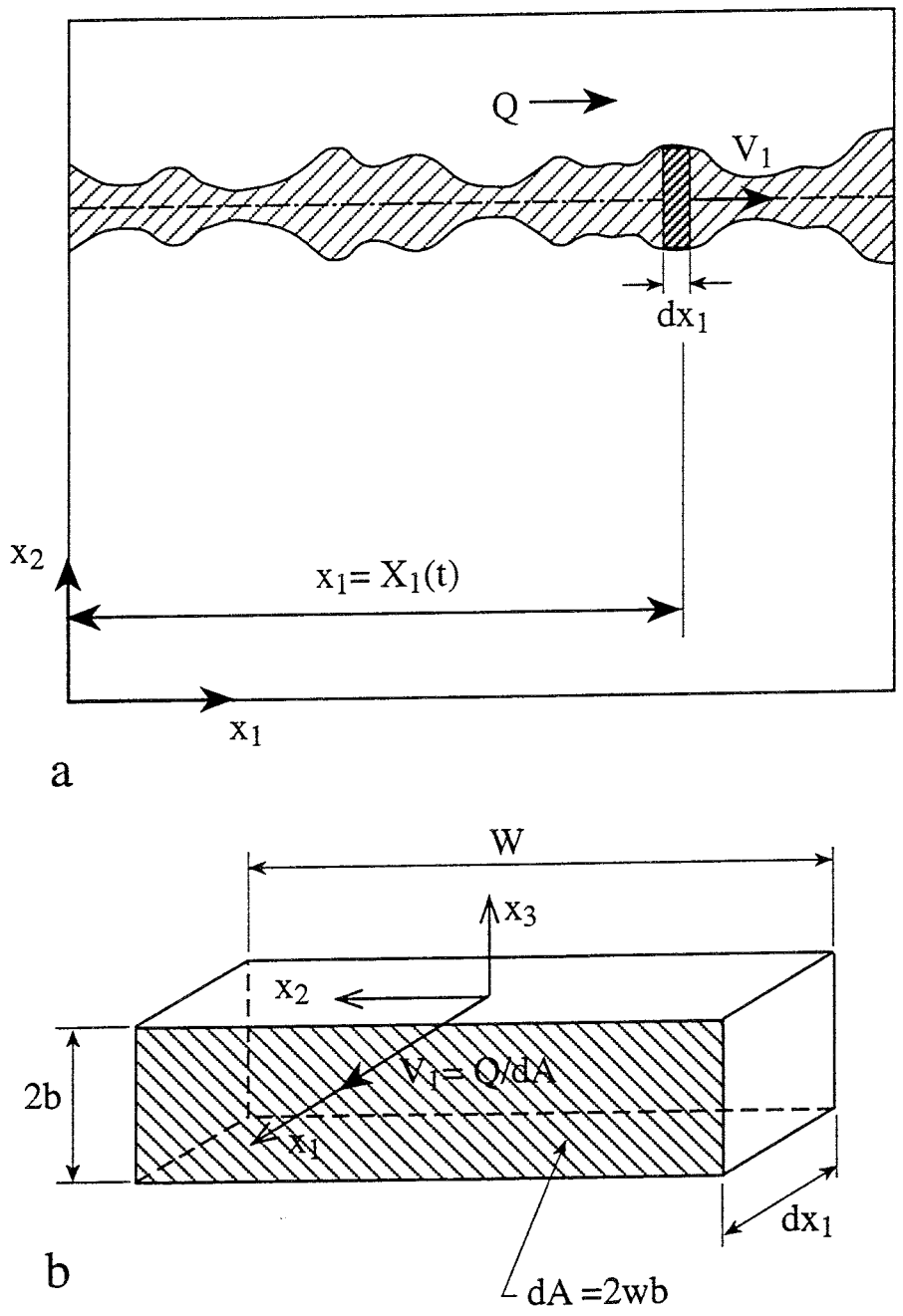

Figure 2.7 *Fracture in $x_1 - x_2$ plane with varying velocity $V_1(x_1)$ along the flow path. b) Elementary volume along the flow path with the cross-sectional area dA indicated by shading.*

3 Theory

3.1 Transport in fractures

Consider a tracer injected into a fracture at $x_1 = 0$ (Figure 2.7a). The tracer is advected by the fluid along a distinct flow path of discharge Q; conservation of fluid mass implies Q =const. The tracer exchanges mass with immobile fluid in the matrix and the solid of the fracture surface.

We denote by C $[ML^{-3}]$ the mobile tracer concentration (in fractures), and by N $[ML^{-3}]$ the immobile tracer concentration (in the rock matrix), where N is defined per unit pore water. The mass balance equations are written along x_1 and x_3 (Figure 2.7b) as

$$\frac{\partial C}{\partial t} + \frac{\partial S}{\partial x_1} = \psi_f \tag{1}$$

$$\frac{\partial N}{\partial t} + \frac{\partial J_m}{\partial x_3} = \psi_m \tag{2}$$

where ψ_f and ψ_m are source terms in the "fracture" (mobile fluid) and the rock "matrix" (immobile fluid/solid), respectively, with dimensions $[MT^{-1}L^{-3}]$; these depend on C, N, their gradients, etc., and on a set of parameters that control the mass transfer and ultimately the retention of the tracer. S and J_m are tracer fluxes in the fracture and the rock matrix, respectively, with dimensions $[MT^{-1}L^{-2}]$.

In order to solve the transport problem, we make the following two assumptions:

(i) Transport in the fractures is by *advection* only, i.e. we neglect the effect of local dispersion, e.g. due to the fluid velocity fluctuations *within* a given flow path; hence

$$S = QC/\mathrm{d}A(x_1) = V_1(x_1)C \tag{3}$$

where $dA(x_1) = 2b(x_1)w(x_1)$ is the cross-sectional area of a flow path at x_1, that is proportional to the "flow porosity," and $V_1 = Q/dA$ is the fluid velocity component parallel to x_1 along a flow path (Figure 2.7a and 2.7b).

(ii) Transport in the rock matrix is by *diffusion* only, i.e. tracer movement in the rock matrix by fluid advection is neglected. Furthermore, we shall consider only the concentration gradients in the rock matrix that are orthogonal to the fracture plane $(x_1 - x_2)$ (Figure 2.7b), and neglect the effect of gradients parallel to the fracture; hence

$$J_m = -D\frac{\partial N}{\partial x_3} \tag{4}$$

with D being the diffusion coefficient in the rock matrix.

In addition to the diffusive mass transfer of the tracer from the flow path to the rock matrix, we consider tracer retention due to *linear equilibrium sorption*, both in the rock matrix and over the contact surface. The source term ψ_f is thereby decomposed as

$$\psi_f = \psi_f^d + \psi_f^s \tag{5}$$

where ψ_f^s is the source component due to equilibrium sorption, and ψ_f^d is the as yet unspecified rate of tracer mass transfer between the flow path and the rock matrix due to diffusion.

3.2 Key processes

Advection

The Lagrangian trajectory of a tracer injected at $t = 0$ at $x_1 = 0$ in the fracture is $X_1(t)$ and is obtained by solving the integral equation $X_1(t) = \int_0^t V_1[X_1(t')]\,dt'$. The advective (groundwater) residence time, τ, is evaluated by inverting, $X_1(t)$, as $\tau = X_1^{-1}(x_1)$, or directly from

$$\tau(x_1) = \int_0^{x_1} \frac{dx_1'}{V_1(x_1')} = \frac{2}{Q}\int_0^{x_1} b(x_1')w(x_1')\,dx_1' \tag{6}$$

where the latter expression is obtained using $V_1 = Q/dA$.

Diffusion

We define the source term for the tracer in the mobile fluid due to diffusive mass transfer as

$$\psi_f^d \equiv \frac{D\theta}{b(x_1)}\frac{\partial N}{\partial x_3} \tag{7}$$

where θ is the matrix porosity assumed spatially uniform. With (5) and (7), the mass balance equations (1) and (2) become

$$\frac{\partial C}{\partial t} + \frac{\partial S}{\partial x_1} = \frac{D\theta}{b(x_1)}\frac{\partial N}{\partial x_3} + \psi_f^s \tag{8}$$

$$\frac{\partial N}{\partial t} = D\frac{\partial^2 N}{\partial x_3^2} + \psi_m \tag{9}$$

Equilibrium sorption

The source term in the fracture and the matrix are respectively written as

$$\psi_f^s \equiv -\frac{\partial C'}{\partial t} \quad ; \quad \psi_m \equiv -\frac{\partial N'}{\partial t} \tag{10}$$

where C' and N' are the sorbed concentrations on the contact surface, and in the rock matrix, respectively; the superscript "s" on ψ_f^s denotes the part of ψ_f due to equilibrium sorption. Hence we can write

$$C' = \frac{K_d^f}{b(x_1)} C \quad ; \quad N' = K_d^m N \tag{11}$$

where K_d^f and K_d^m are the distribution coefficients on the fracture surface and in the matrix, respectively.

Coupling equilibrium sorption with matrix diffusion then yields mass balance equations in the form

$$R_f(x_1)\frac{\partial C}{\partial t} + \frac{\partial S}{\partial x_1} = \frac{\theta D}{b(x_1)}\frac{\partial N}{\partial x_3} \tag{12}$$

$$\frac{\partial N}{\partial t} = \frac{D}{R_m}\frac{\partial^2 N}{\partial x_3^2} \tag{13}$$

where

$$R_f \equiv 1 + \frac{K_d^f}{b(x_1)} \quad ; \quad R_m = 1 + K_d^m \tag{14}$$

Mass flux formulation

In the following, similar steps are used as those presented in *Cvetkovic* (1991). Substituting (3) into (12), and multiplying (12) and (13) by V_1, we obtain

$$R_f(x_1)\frac{\partial S}{\partial t} + V_1(x_1)\frac{\partial S}{\partial x_1} = \frac{\theta D}{b(x_1)}\frac{\partial N^*}{\partial x_3} \tag{15}$$

$$\frac{\partial N^*}{\partial t} = \frac{D}{R_m}\frac{\partial^2 N^*}{\partial x_3^2} \tag{16}$$

where

$$N^* \equiv N V_1$$

N^* does not have an apparent physical interpretation and can be considered as an auxiliary quantity; our prime objective is to solve (15)-(16) for the tracer mass flux in the fracture, S.

3.3 Solution for the flux

In order to solve (15)-(16), the initial and boundary conditions are defined as follows. We consider a pulse injection

$$S(0,t) = \rho_0 \delta(t) \tag{17}$$

where ρ_0 $[ML^{-2}]$ is the density of the injected tracer, defined as mass per unit injection area. Initially, both the fracture and the matrix do not contain any tracer; hence $C(x_1,0) = N(x_1,0) = 0$, or after multiplication by V_1,

$$S(x_1,0) = N^*(x_1,0) = 0 \tag{18}$$

Furthermore, we assume the matrix to be large (unbounded). An additional condition is $C = N$ for $x_3 = 0$ (Figure 2.7b), or after multiplication by V_1,

$$S = N^* \qquad \text{for} \qquad x_3 = 0 \tag{19}$$

where C (i.e., S) is independent of x_3.

The solution of (15) and (16) for S is obtained using Laplace transform as (Appendix, 9.1)

$$S(x_1,t;\tau) = \rho_0 \gamma[t,\tau;\beta(x_1)] \tag{20}$$

where

$$\gamma(t,\tau;\beta) \equiv \frac{H(t-\tau-K_d^f\beta)\,\kappa\beta}{2\sqrt{\pi}(t-\tau-K_d^f\beta)^{3/2}} \exp\left[\frac{-\kappa^2\beta^2}{4(t-\tau-K_d^f\beta)}\right] \tag{21}$$

and $H()$ is the Heaviside step function. In addition to the water residence time, τ, the other two parameters that control γ in (21) are κ and β. κ is a constant defined by

$$\kappa \equiv \theta\sqrt{DR_m} \tag{22}$$

whereas β is

$$\beta(x_1) = \int_0^{x_1} \frac{dx_1'}{V_1(x_1')b(x_1')} \tag{23}$$

Using $Q = V_1\,dA = V_1 2bw$, we can write

$$\beta(x_1) \equiv \frac{1}{q}\int_0^{x_1} w(x_1')dx_1' \tag{24}$$

where $q = Q/2$ is the fluid discharge through the half-fracture area bw. Thus the parameter β is equal to the total area in contact with the rock matrix, normalized by

the volumetric water flux, q. If the width is constant w =const., then $\beta = wx_1/q$ is constant along a flow path, and we recover the case commonly used in analytical models of diffusive mass transfer in fractures (e.g., *Moreno et al.*, 1995). For a similar set of equations as (12) and (13), *Lee et al.* (1990) have presented a solution expressed in terms of the concentration C where additional spatial variability in the diffusion coefficient may be accounted for.

If the sorption on the contact surface is negligible, $K_d^f = 0$ and

$$\gamma(t,\tau;\beta) = \frac{H(t-\tau)\,\kappa\beta}{2\sqrt{\pi}(t-\tau)^{3/2}} \exp\left[\frac{-\kappa^2\beta^2}{4(t-\tau)}\right] \tag{25}$$

In (21) and (25), β is the critical parameter that characterizes retention due to diffusion into the rock matrix, as well as due to sorption along the contact surface. We emphasize that the results (21) and (25) are independent of the simplified flow path geometry, and are applicable to two-dimensional flow in a fracture with variable aperture. This can be shown using the transformations of *Cvetkovic and Dagan* (1994) and *Dagan and Cvetkovic* (1996), as demonstrated in *Cvetkovic and Dagan* (in preparation) for sorption in heterogeneous granular aquifers.

The water residence time to the control plane at x_1 is given by (6), which using $q = Q/2$ is expressed as

$$\tau(x_1) = \frac{1}{q}\int_0^{x_1} b(x_1')w(x_1')\,dx_1' \tag{26}$$

Note that from (24) and (26), a definition of an effective fracture half-aperture is obtained as

$$b_e \equiv \frac{\tau\,(x_1)}{\beta\,(x_1)} \tag{27}$$

The half-aperture (27) is a mass balance aperture following the notation introduced by *Tsang* (1992).

3.4 Mass flux moments

In order to evaluate the expected tracer mass flux at the control plane x_1, we observe that both the parameter β and the water residence time τ are random variables. In general, β and τ will be correlated since both parameters are dependent on the RSF w, cf. (24) and (26). Thus we define a joint pdf $h(\tau,\beta;x_1)$, and the expected tracer flux is obtained as

$$< S\,(t;x_1) > \equiv \bar{S}(t;x_1) = \int_0^\infty \int_0^\infty \rho_0\gamma(t,\tau,\beta)h(\tau,\beta;x_1)d\tau\,d\beta \tag{28}$$

and the variance of the tracer flux as

$$\sigma_S^2(t;x_1) = \int_0^\infty \int_0^\infty \rho_0^2 \left[\gamma(t,\tau,\beta)\right]^2 h(\tau,\beta;x_1)\, d\tau d\beta - \left[\overline{S}(t;x_1)\right]^2 \tag{29}$$

If β and τ are assumed independent (uncorrelated) random variables, the joint pdf may be written as $h(\tau,\beta;x_1) = g(\tau;x_1)\, g(\beta;x_1)$, where g is a univariate pdf. Using the univariate pdf for β, we can define the mass flux moments for the simplifying case where we assume τ to be a constant or effective value $\overline{\tau}$. The expected value is then obtained as

$$\bar{S}(t;x_1,\overline{\tau}) = \int_0^\infty \rho_0 \gamma(t,\beta;\overline{\tau}) g(\beta;x_1)\, d\beta \tag{30}$$

and the variance as

$$\sigma_S^2(t;x_1,\overline{\tau}) = \int_0^\infty \rho_0^2 \left[\gamma(t,\beta;\overline{\tau})\right]^2 g(\beta;x_1)\, d\beta - \left[\bar{S}(t;x_1,\overline{\tau})\right]^2 \tag{31}$$

Analogous equations using g may be derived for the case where an effective value $\overline{\beta}$ is defined and the random variable is τ. The pdf $g(\tau;x_1)$ is then simply the fluid residence time distribution for an ensemble of flow paths obeying the specified half-aperture and width statistics.

4 Visual representation of flow path structure

In the following we assume specific distributions and correlation structures for the half-aperture and width RSFs, and visually compare the resulting flow paths. In the sequel, we shall use the flow path statistics to evaluate the mass flux moments derived in the previous section.

For illustrative purposes, we assume that the half-aperture and width along a flow path are lognormally distributed according to

$$b(x_1) = b_G \exp[Y(x_1)] \quad ; \quad w(x_1) = w_G \exp[\alpha Y(x_1) + Z(x_1)] \tag{32}$$

where Y and Z are independent, normally distributed RSFs of zero mean and given covariance, and b_G and w_G are the geometric means of b and w, respectively. The parameter α is the slope of the straight line expressing perfect correlation between $\ln b$ and $\ln w$ if the variance of Z is zero, i.e. $\sigma_Z^2 = 0$. We shall assume $-1 \leq \alpha \leq 1$. The coefficient of correlation between b and w is thus a function of α and of the relative difference in variability between Y and Z. In the present context the specific statistical model of the flow path geometry is generic.

In a computational representation, the flow path is constructed from a series of elements of the type shown in Figure 2.7b. By using a small enough discretization dx_1 along the flow path, a flow channel with seemingly continuous change in aperture and width is obtained. A sketch of a prototype of a flow path is presented in Figure 2.7a in a planar view.

In order to construct a flow path, spatial correlation models for the RSFs have to be assumed. We consider first an exponential spatial correlation model

$$\rho(r) = \exp(-r/a) \tag{33}$$

where ρ is the correlation coefficient, r is the separation distance and a is the correlation distance of the variable of interest, i.e. Y or Z, in the x_1 direction; for this model, the correlation distance is equal to the integral scale I. The resulting correlation function $C(r)/C(0) = \exp(-r/a)$ is plotted in Figure 4.1 for different correlation distances a. It is observed that the horizontal axis is normalized with the correlation distance $a = a_r$, where the subscript r denotes a reference case where the total length of the flow path is $10a_r$. For this case, the correlation is practically zero at a distance $x_1 = 3a_r$. This distance is called the correlation range. When the correlation distance is increased to $a = 2a_r$, the correlation function has a longer range. The opposite is true when the correlation distance is reduced to $a = 0.5a_r$.

A different correlation model is the Gaussian model which is given by

$$\rho(r) = \exp\left(-r^2/a^2\right) \tag{34}$$

In Figure 4.1 the correlation function is presented for the Gaussian model with a correlation length $a = \sqrt{3}a_r$. The choice of a implies that the range over which values are correlated is the same as for the exponential model with $a = a_r$; the range of the Gaussian model is $\sqrt{3}a$. However, the Gaussian model has stronger correlation for distances shorter than the correlation range, and weaker correlation only for distances longer than the correlation range.

In Figure 4.2a-4.2f several realizations of different flow path geometries are presented. In each figure, five individual realizations are plotted where the width is given by (32). The horizontal axis in a figure is the flow path distance normalized with the correlation distance of the reference case. On the vertical axis the flow path width is represented normalized with the geometric mean width, i.e. the distance between two closely adjacent streamlines represents $w(x_1)/w_G$. The scale of the vertical axis is identical in all figures; thus a quantitative comparison is possible.

In Figure 4.2a the result of five realizations with the width statistic given by $\alpha = 0$ and $\sigma_Z^2 = 0.15$ is presented. The flow paths are characterized by fairly erratic shapes; the width fluctuations are induced by the short integral scale (I_Z) relative to the length scale of the flow path. Increasing the integral scale by a factor two (Figure 4.2b), or decreasing the integral scale by a factor two (Figure 4.2c), results in smoother or even more erratic flow paths, respectively. This can also be deduced from the correlation functions in Figure 4.1; a shorter correlation length results in a correlation function with steeper drop.

When the width is correlated to the half-aperture through the parameter α, a more erratic flow path also emerges. This is due to the fact that Y and Z are independent RSFs. In Figure 4.2d it is assumed that $\alpha = -1$ and that both the Y- and Z-statistics are identical to the Z-statistic in Figure 4.2a. The reason for assuming a negative α is that for large aperture values one may expect that the width of the flow path decreases due to continuity.

More erratic flow paths are also produced by increasing the width variance; in Figure 4.2e five flow paths are presented for a case where the variance of Z is increased by a factor five, i.e. $\sigma_Z^2 = 0.75$. Furthermore, a smoother and more continuous flow path can be obtained by a spatial correlation function with a higher degree of correlation for shorter separation distances, e.g. the Gaussian correlation model presented in Figure

4.1. The resulting flow paths for the Gaussian model are presented for a case with $\sigma_Z^2 = 0.75$ and $a = \sqrt{3}a_r$ in Figure 4.2f.

Finally we note that the kinematic model of a flow path proposed by O. Olsson in *Olsson et al.* (1995) (Figure 2.5) is obtained by assuming the correlation coefficient for both b and w in the form

$$\rho(r) = (1 - r/L) \quad \text{for} \quad r < L \tag{35}$$

and $\rho = 0$ for $r > L$, where $L \equiv L_i$, i.e. the segments are assumed constant. If the segment length is variable according to a given distribution, $\rho(r)$ takes a more complicated form (see e.g. *Cvetkovic et al.*, 1991).

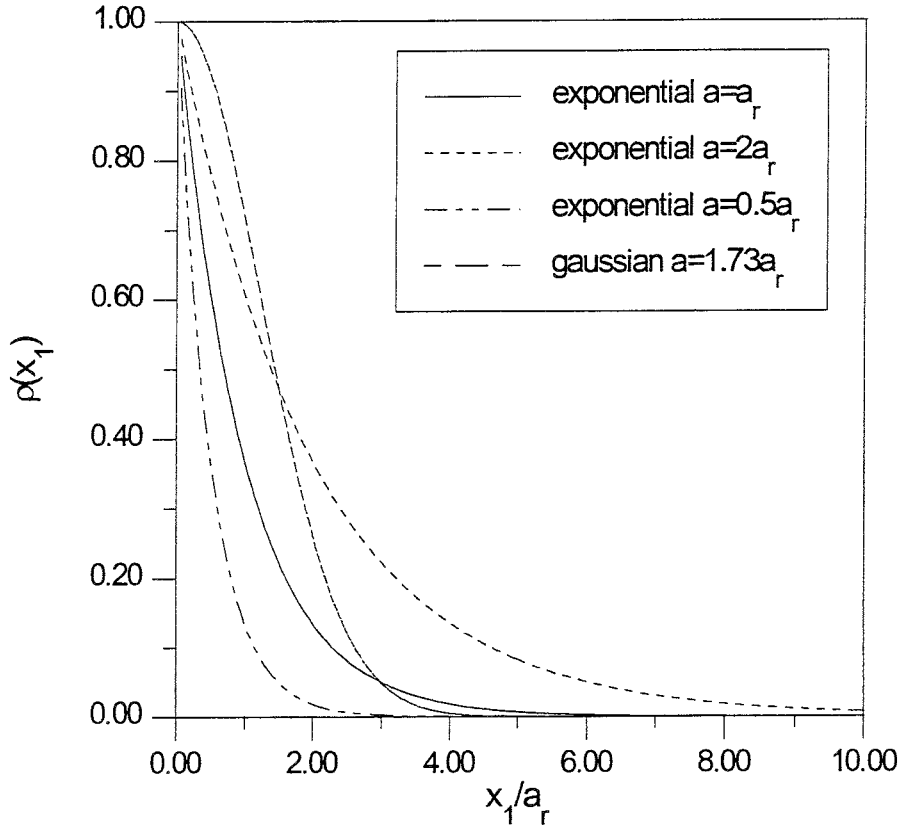

Figure 4.1 *Correlation function for exponential and Gaussian models. Observe that distance is normalized with the correlation length* $a = a_r$ *of the reference case.*

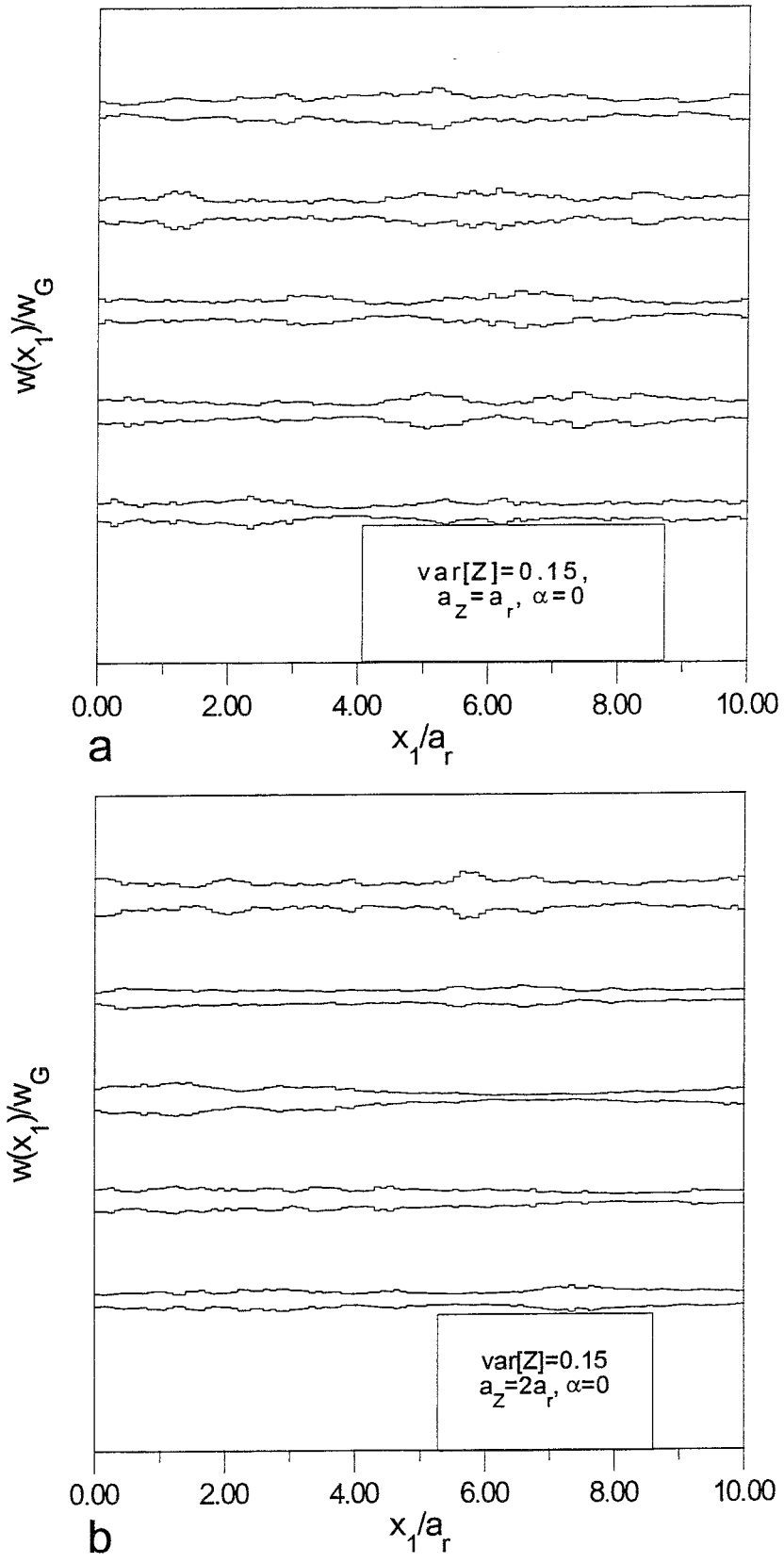

Figure 4.2 *Five realizations of the prototype flow path width* $w(x_1)$ *for a) reference case, and for b)* $a_Z = 2a_r$.

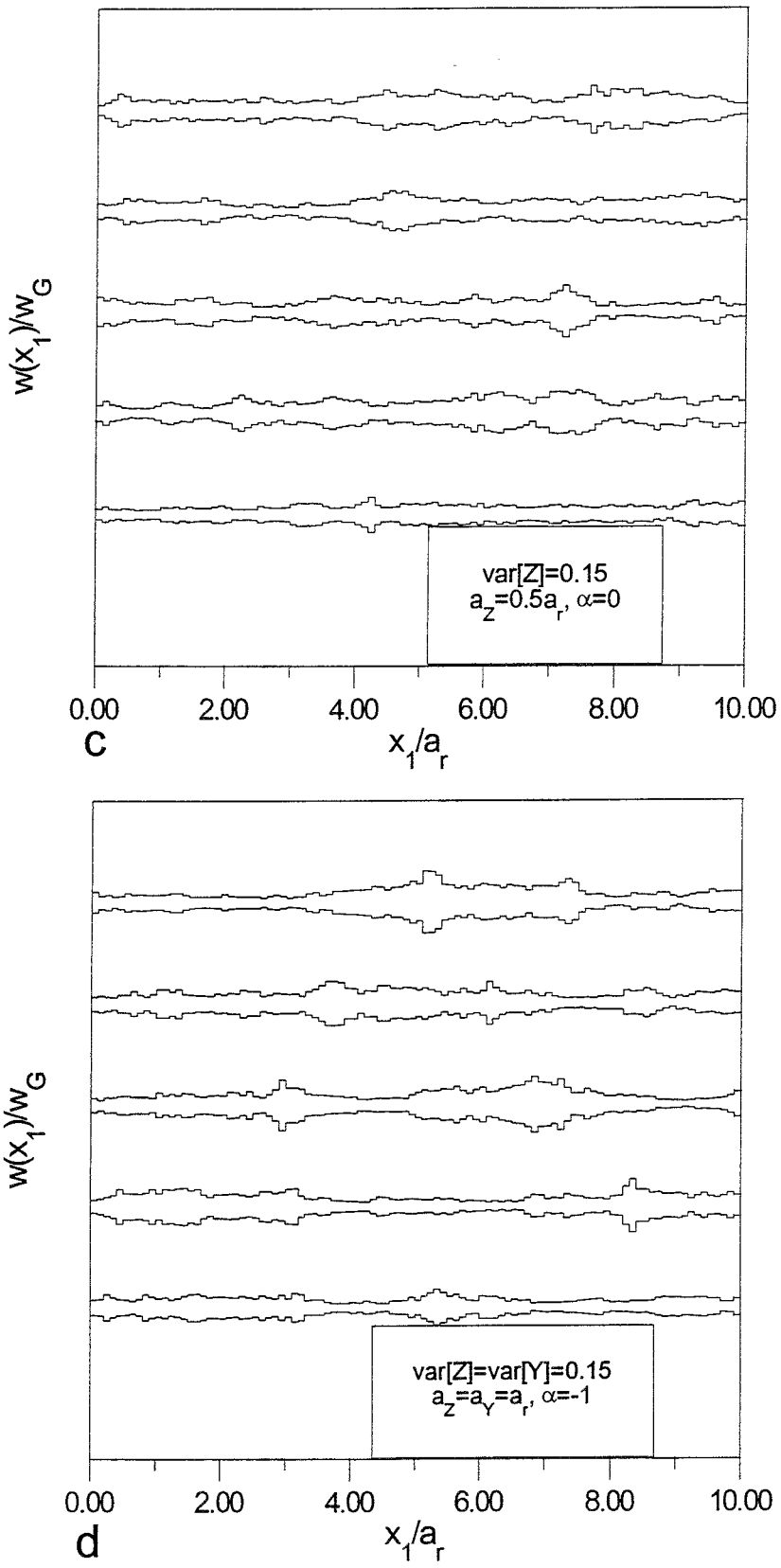

Figure 4.2 *Five realizations of the prototype flow path width* $w(x_1)$ *for c)* $a_Z = 0.5a_r$*, and for d)* $\alpha = -1$.

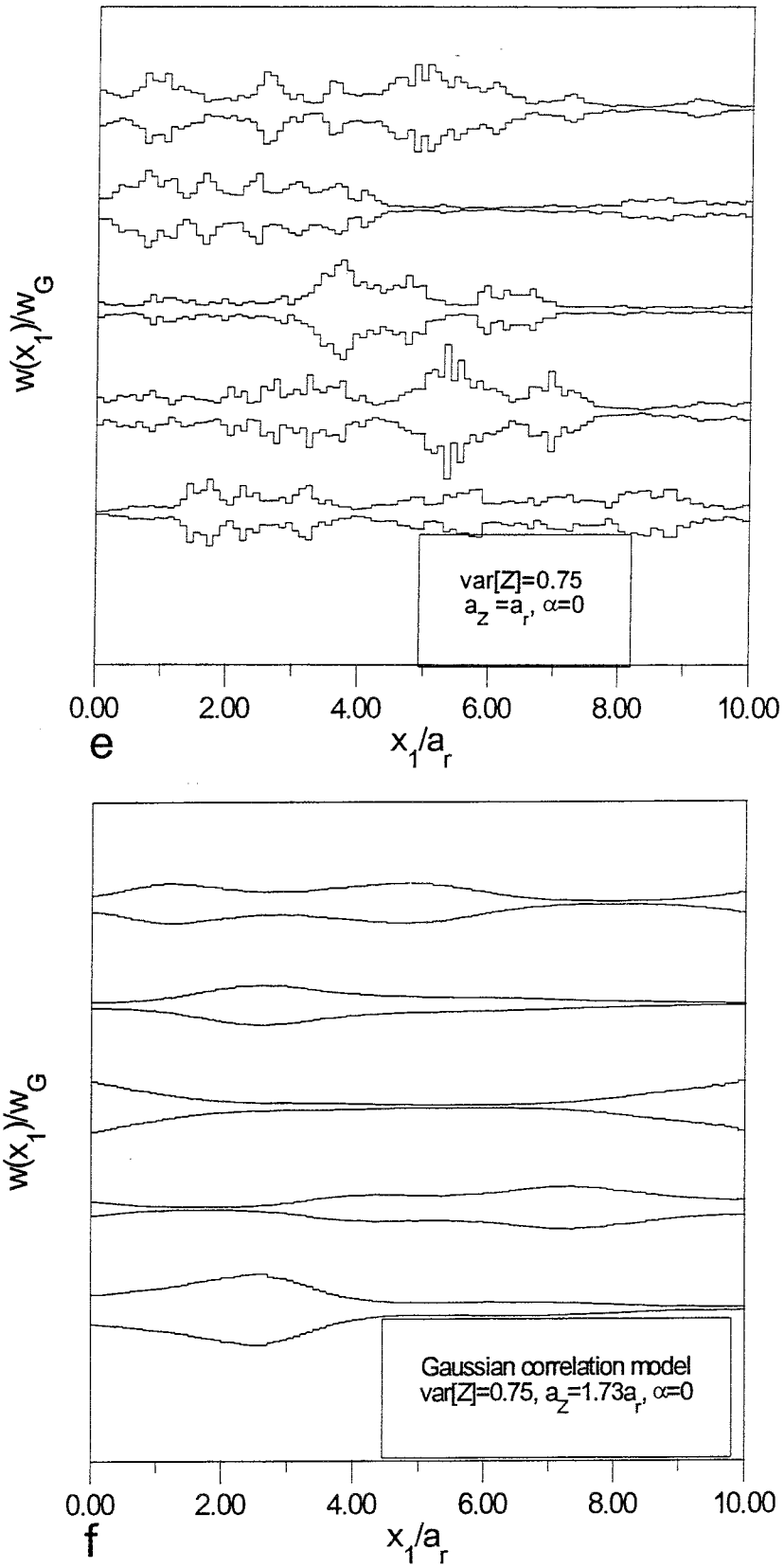

Figure 4.2 *Five realizations of the prototype flow path width* $w(x_1)$ *for e)* $\sigma_Z^2 = 0.75$*, and f) Gaussian correlation model with* $\sigma_Z^2 = 0.75$*.*

5 Mean and variance of mass flux

In the present section, the resulting mass flux moments will be evaluated based on β and τ statistics for the flow path configurations analyzed above. If both β and τ are considered random, the mass flux moments are given by (28) and (29); if only β or τ is random, expressions of the form (30) and (31) yield the expected mass flux and mass flux variance. For comparative purposes, we shall separately analyze the mass flux moments when only β is variable while $\tau = \overline{\tau}$ is constant, and when only τ is variable and $\beta = \overline{\beta}$ is constant. We shall also compare both cases with the "deterministic" case, when the variability in both τ and β is neglected, and constant (best estimates) are used as $\beta = \overline{\beta}$ and $\tau = \overline{\tau}$.

The ensemble moments of β and τ are derived analytically based on the underlying statistics of Y and Z. The derivations, which are presented in the Appendix (9.2), are exact and provide integral expressions for the variances and covariance of β and τ.

The first two moments of β are obtained as (Appendix, 9.2)

$$\overline{\beta}(x_1) = \frac{w_G x_1}{q} \exp\left[\alpha^2 \frac{\sigma_Y^2}{2} + \frac{\sigma_Z^2}{2}\right] \tag{36}$$

and

$$\begin{aligned} \sigma_\beta^2(x_1) &= \frac{2w_G^2}{q^2} \exp\left[\alpha^2 \sigma_Y^2 + \sigma_Z^2\right] \\ &\cdot \int_0^{x_1} (x_1 - x) \left[\exp\left[\alpha^2 C_Y(x) + C_Z(x)\right] - 1\right] dx \end{aligned} \tag{37}$$

where C_Y and C_Z are given in (33) or (34).

The first two moments of the residence time, τ, are obtained as (Appendix, 9.2)

$$\overline{\tau}(x_1) = \frac{b_G w_G x_1}{q} \exp\left[\frac{(\alpha+1)^2 \sigma_Y^2}{2} + \frac{\sigma_Z^2}{2}\right] \tag{38}$$

and

$$\begin{aligned} \sigma_\tau^2(x_1) &= \frac{2b_G^2 w_G^2}{q^2} \exp\left[(\alpha+1)^2 \sigma_Y^2 + \sigma_Z^2\right] \\ &\cdot \int_0^{x_1} (x_1 - x) \left[\exp\left[(\alpha+1)^2 C_Y(x) + C_Z(x)\right] - 1\right] dx \end{aligned} \tag{39}$$

respectively. The behavior of the β and τ moments for width and aperture statistics pertinent to the flow paths of the previous section is discussed in the Appendix (9.2).

5.1 Effect of β variability with $\tau = \overline{\tau}$

In Figure 5.1a results are presented for a case where the β-distribution is assumed lognormal with moments defined in (36) and (37) with $\sigma_Y^2 = \sigma_Z^2 = 0.15$, $\alpha = 0$, and with $\tau = \overline{\tau}$ given by (38). *Hakami and Larsson* (in press) obtained a similar fracture aperture variability when analyzing a well mated joint at the Äspö Hard Rock Laboratory.

First we assume sorption in the matrix only such that the solution for γ is given by (25). The used sorption coefficient κ corresponds e.g. to a case with $K_d = 1$ m^3/kg, ρ =2400 kg/m^3, $\theta = 0.001$ and $D = 2.5 \times 10^{-11}$ m^2/s where K_d^m in (14) is defined as $K_d^m = K_d \rho (1-\theta)/\theta$ and K_d and ρ are a volumetric sorption (distribution) coefficient and specific rock matrix density, respectively. Figure 5.1a is normalized such that the conservative breakthrough occurs at $tq/(b_G w_G x_1) = \exp\left[(\alpha+1)^2 \sigma_Y^2/2 + \sigma_Z^2/2\right]$. The light solid line in the figure is the normalized expected tracer flux, the dotted lines are the normalized expected tracer fluxes plus/minus one standard deviation. The thick solid line is the normalized deterministic tracer flux (25) evaluated with a constant $\tau = \overline{\tau}$ and $\beta = \overline{\beta}$, where $\overline{\beta}$ is given by (36). It is observed that the deterministic and expected tracer fluxes practically coincide; i.e. for the given variability in β, almost the same tracer flux is obtained if (25) is evaluated using the expected value of β or if the expectation operation is carried out using the pdf of β (30). However, a mass flux uncertainty exists for the early breakthrough and is quantified through the mass flux standard deviation. For larger times the prediction uncertainty is negligible.

In Figure 5.1b the normalized parameter κ is reduced by approximately a factor 3.2, i.e. the change in R_m is $3.2^2 \approx 10$. Compared to the case with higher matrix sorption in Figure 5.1a, the breakthrough occurs earlier (observe the logarithmic time scale and larger γ scale in Figure 5.1b). Furthermore, comparing the magnitude of the fluxes in Figure 5.1a and 5.1b, the peak flux and uncertainty around the peak flux are higher for the low sorption case in Figure 5.1b. However, the flux coefficient of variation, $\mathrm{CV}_\gamma = \sigma_\gamma/\overline{\gamma}$, at the peak is approximately the same for both cases.

In Figure 5.1c, a case with high variability in β according to $\sigma_Y^2 = \sigma_Z^2 = 0.75$ and $\alpha = 0$ is presented. The normalized κ-value is the same as in Figure 5.1a. For the case in Figure 5.1c, a clear discrepancy between the deterministic and expected fluxes is observed. The effect of the introduced variability is an enhanced and earlier peak flux. Thus, if one neglects spatial variability in β, one may underestimate the magnitude of the peak flux and overestimate the time of the peak flux. Furthermore, the flux coefficient of variation, CV_γ, around the peak is larger for the case in Figure 5.1c as compared to

the low variability case in Figure 5.1a. This implies that the prediction uncertainty is larger for the case with more spatial variability. The reason for the lower deterministic and expected fluxes in Figure 5.1c as compared to the low variability case in Figure 5.1a are the increases in the first moments of β and τ as given by (36) and (38), respectively.

In Figure 5.1d, a case with combined sorption in the matrix and on the fracture surface is presented. For combined sorption, γ is evaluated according to (21). The β-statistics and matrix sorption characteristics are the same in Figure 5.1d as in Figure 5.1c; the surface sorption is defined through a normalized surface related distribution coefficient $K_a/b_G \equiv K_d^f/b_G = 9.6$. For a geometric half-aperture of 0.1 mm, the surface sorption coefficient would be approximately $K_a = 1$ mm. *Neretnieks et al.* (1982) have reported K_a values of this magnitude for both strontium and cesium on Stripa granite. Comparing the results in Figure 5.1c and 5.1d, the effect of the additional surface sorption is observed in the deterministic tracer flux as a delay of approximately 10 normalized time units. However, for the expected tracer flux, the additional surface sorption does not only imply a delay, but also a reduction in the peak flux. Likewise, a reduction in the flux variance is also observed for the surface sorption case. Thus, for the case of combined sorption, the underestimation of the peak flux when neglecting variability in β is smaller than for the case of sorption in the matrix only (Figure 5.1c). The overestimation of the time of the peak arrival however is still apparent.

5.2 Effect of τ variability with $\beta = \overline{\beta}$

To elucidate the effect of τ variability as compared to β variability, we assume a log-normal pdf for τ with moments defined in (38) and (39), and compute the mass flux moments from equations similar to (30) and (31) but with τ as the random variable and with $\beta = \overline{\beta}$. The first moment of the pdf for τ is equal to the effective τ-value used in the previous section where β was assumed the random variable. In Figure 5.2a, results corresponding to the variability and mass transfer in Figure 5.1b are presented, i.e. $\sigma_Y^2 = \sigma_Z^2 = 0.15$, $\alpha = 0$, and $\kappa\sqrt{w_G x_1/(q b_G)} = 2.9$. Only an insignificant discrepancy between the deterministic and expected mass flux is observed around the peak flux; however, compared to the case with small variability in β in Figure 5.1b, the expected mass flux is primarily manifested by early mass arrival prior to the conservative mean arrival time $\overline{\tau}$. Furthermore, the uncertainty envelopes are of a smaller magnitude, with a smaller CV_γ, in Figure 5.2a than in Figure 5.1b. Thus, spatial variability in flow path aperture and width are manifested quite differently when the mass flux moments are evaluated with $\tau = \overline{\tau}$ (Figure 5.1b) or with $\beta = \overline{\beta}$ (Figure 5.2a). Specifically, the

β-pdf has a much larger influence on the mass flux uncertainty than the corresponding residence time pdf has.

In Figure 5.2b the residence time variability has been increased according to $\sigma_Y^2 = \sigma_Z^2 = 0.75$ and $\alpha = 0$. The increased variability results in an expected peak flux which is decreased relative to the deterministic flux (i.e. with $\beta = \overline{\beta}$ and $\tau = \overline{\tau}$). A significant part of the expected flux lies prior to the deterministic flux. The effect of the residence time variability on the expected flux is thus clearly seen in Figure 5.2b: a wider distribution in time with a reduced peak. Furthermore, even for the case with high variability in τ presented in Figure 5.2b, the CV_γ at the peak is lower than for the case with low variability in β (Figure 5.1b). This further emphasizes the stronger effect of the β-variability on the mass flux prediction uncertainty.

The effect of an increase in κ is a deterministic mass flux with a delayed and diminished peak. Moreover, with increasing κ-values, the flux variance and the discrepancy between the deterministic and expected tracer fluxes diminish. Thus, with increasing sorption in the matrix, the effect of residence time variability becomes smaller on the prediction uncertainty. Specifically, if the normalized κ-value in Figure 5.2b would be increased to 9.3 corresponding to the cases in Figure 5.1a and 5.1c, the mass flux variance would be reduced to practically zero, and the expected and deterministic fluxes would coincide completely.

A more general analysis of flow path variability would be based on hypothesizing a bivariate distribution for τ and β and evaluating the mass flux moments using (28) and (29); such computations are not pursued in the present study.

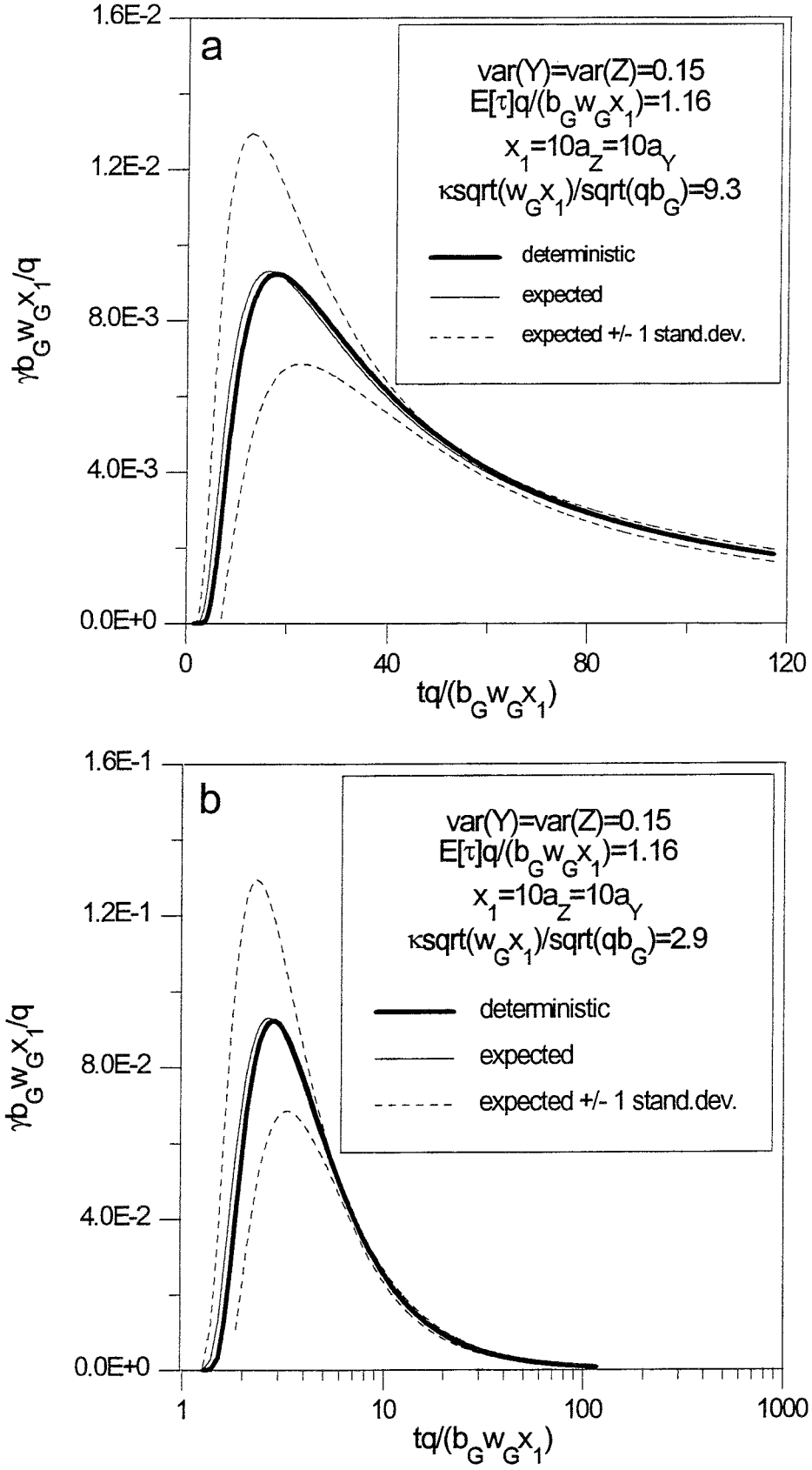

Figure 5.1 *Flux estimates for a) low variability in β and high matrix sorption, and b) low variability in β and low matrix sorption.*

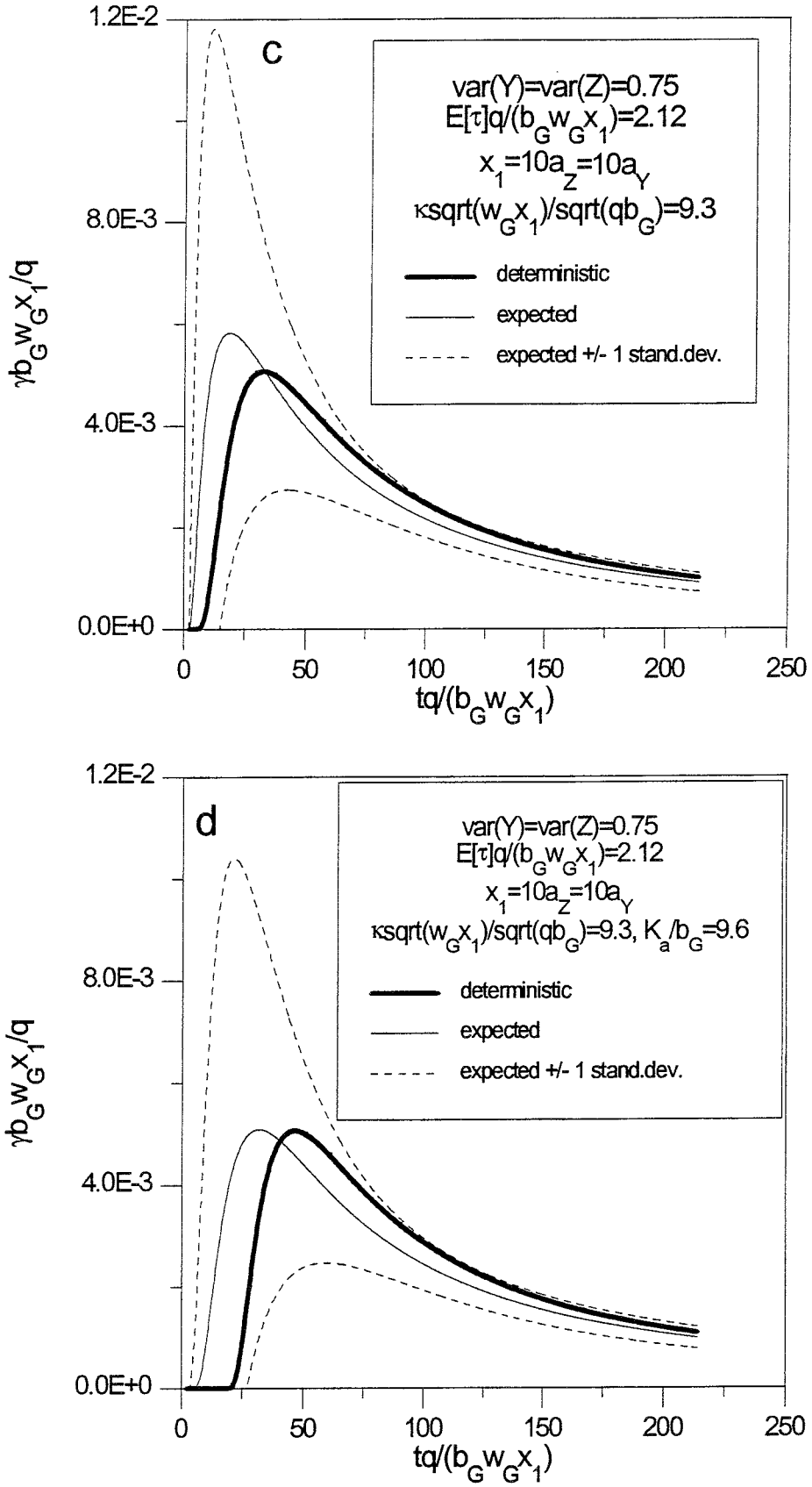

Figure 5.1 *Flux estimates for c) high variability in β and high matrix sorption, and d) high variability in β, high matrix sorption and surface sorption.*

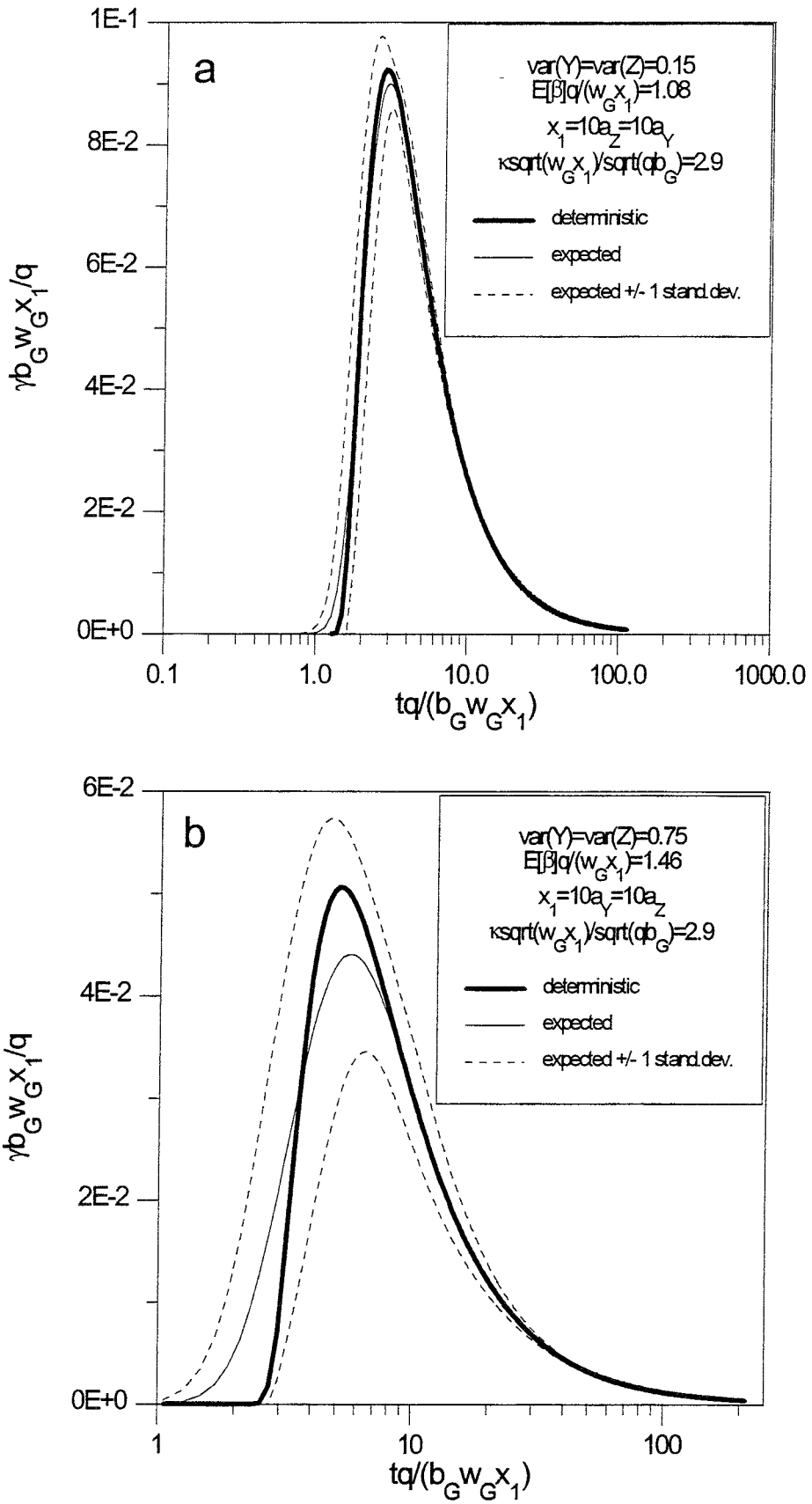

Figure 5.2 *Flux estimates for a) low variability in τ and low matrix sorption, and b) high variability in τ and low matrix sorption.*

6 Cumulative mass arrival

Integrating (25) over time, we obtain the cumulative mass arrival in a dimensionless form, ϕ, as

$$\phi(t,\tau) = \int_0^t \gamma(t',\tau;\beta)\,dt' = \text{erfc}\left[\frac{1}{2}\left(\frac{1}{t-t_0-\tau}\right)^{1/2}\kappa\beta\right] \tag{40}$$

Thus $0 < \phi < 1$ quantifies the fraction of the released tracer mass as a function of the clock time t (from closure), the release time t_0, and the groundwater/advective residence time, τ. Note that (40) is applicable to continuous injection at a constant rate; ϕ is then the relative concentration.

The two controlling parameters are κ and β; we assume that κ is known exactly, and τ, β and t_0 are known statistically. In order to more clearly focus on the effect of retention, we simplify the problem by setting $t_0 = 0$, i.e. assuming that the release of radionuclides coincides with repository closure. As before, we restrict our discussion to the case where decay is negligible.

Let t_ϕ denote the time of arrival of a particular mass fraction, ϕ. We evaluate t_ϕ from

$$F \equiv \text{erfc}^{-1}(\phi) = \frac{\beta\kappa}{2\sqrt{t_\phi - \tau}} \tag{41}$$

as

$$t_\phi = \tau + \frac{\kappa^2\beta^2}{4F^2} \tag{42}$$

where erfc^{-1} denotes the inverse of the complementary error function, and ϕ is specified.

The mass fraction arrival time t_ϕ is a random variable due to the randomness of the advective travel time τ and the parameter β. We proceed to compute the first two moments of t_ϕ as

$$\overline{t}_\phi = \overline{\tau} + \frac{\kappa^2}{4F^2}\,\overline{\beta^2} \tag{43}$$

$$\sigma^2_{t_\phi} \equiv \overline{t^2_\phi} - \overline{t}^2_\phi = \sigma^2_\tau + \frac{\kappa^2}{2F^2}\left(\overline{\beta^2\tau} - \overline{\beta^2}\,\overline{\tau}\right) + \frac{\kappa^4}{16F^4}\left(\overline{\beta^4} - \overline{\beta^2}^2\right) \tag{44}$$

where σ^2_τ is the nonreactive tracer (or groundwater) residence time variance. When matrix diffusion is not present, i.e. $\kappa = 0$, the moments are reduced to the nonreactive travel time moments $\overline{\tau}$ and σ^2_τ, respectively. Note that the variance of t_ϕ for $\kappa \neq 0$ depends on the fourth-order moment of β, as well as on the higher-order cross-moment between β and τ. These moments are evaluated in the Appendix (9.3) for the kinematic flow path introduced in Section 2.3 using a first-order expansion technique.

In Figure 6.1 the coefficient of variation CV_{t_ϕ} is presented for different flow path configurations and for a few different values of κ. The results in Figure 6.1a of $CV_{t_{50}}$ (where t_{50} implies t_ϕ for $\phi = 50\%$) for different flow path statistics show similar features as the results for CV_β and CV_τ in Figure A1a and A1b, respectively of the Appendix (9.2). Specifically, CV_{t_ϕ} decreases with distance x; furthermore, an increased correlation distance a_Z, or simultaneously increased variances of σ_Y^2 and σ_Z^2, yields higher CVs. Contrary to the CVs in Figure A1, a pronounced non-linearity is observed for short distances, i.e. $x_1 < a_\tau$. The non-linearity, which results from the higher-order moments included in $\sigma_{t_\phi}^2$, is particularly noticeable for the case with $\alpha = -1$.

In section 5 the relatively stronger influence of variability in β than variability in τ on the mass flux prediction uncertainty was qualitatively assessed through visual comparison of different variability cases. In (44) this influence is explicitly stated through the included higher-order moments of β when $\kappa \neq 0$. Specifically, for a case with $\sigma_Y^2 = 0.75$, $\sigma_Z^2 = 0.15$ and $\alpha = 0$, thus resulting in a higher τ-variability and the same β-variability as in the reference case, the same CV_{t_ϕ} is observed as for the reference case (Figure 6.1a). With $\sigma_Y^2 = 0.15$, $\sigma_Z^2 = 0.75$ and $\alpha = 0$, the same CV_{t_ϕ} is observed as for the case with increased variance in both σ_Y^2 and σ_Z^2 (Figure 6.1a). These features follow from the fact that the moments of β, which dominate $\sigma_{t_\phi}^2$, depend on Z only when $\alpha = 0$. In Figure A1b of the Appendix (9.2) an increase in CV_τ is observed when either σ_Y^2 or σ_Z^2 is increased. For the simplified flow geometry assumed, the prediction uncertainty of the nonreactive travel time τ depends on both aperture and width variability. The prediction uncertainty of the cumulative reactive arrival time t_ϕ depends more strongly on the width variability alone.

In Figure 6.1b the effect of κ on CV_{t_ϕ} is illustrated. Increasing κ-values imply successively higher prediction uncertainties; however, for longer travel distances, i.e. $x_1 > 3a_\tau$, the CV_{t_ϕ}-values converge at a level above the corresponding nonreactive $CV_{t_\phi} \equiv CV_\tau$ given by $\kappa = 0$. Thus, the prediction uncertainty of the nonreactive travel time τ is smaller than the prediction uncertainty of the reactive arrival time t_ϕ. The implications of assuming an effective β-value (neglecting the β-variability) may thus be unconservative in performance assessment applications. The results in Figure 6.1b support the findings in Section 5.1; i.e. the flux coefficient of variation at a normalized distance of 10 was shown to be approximately independent of the normalized sorption parameter.

The difference in CV_τ between Figure 6.1b and the corresponding case in Figure A1b of the Appendix (9.2) is a result of the first-order approximation utilized in the

calculations in Figure 6.1b. A more thorough assessment of effects caused by the first-order approximation is pursued in the Appendix (9.3).

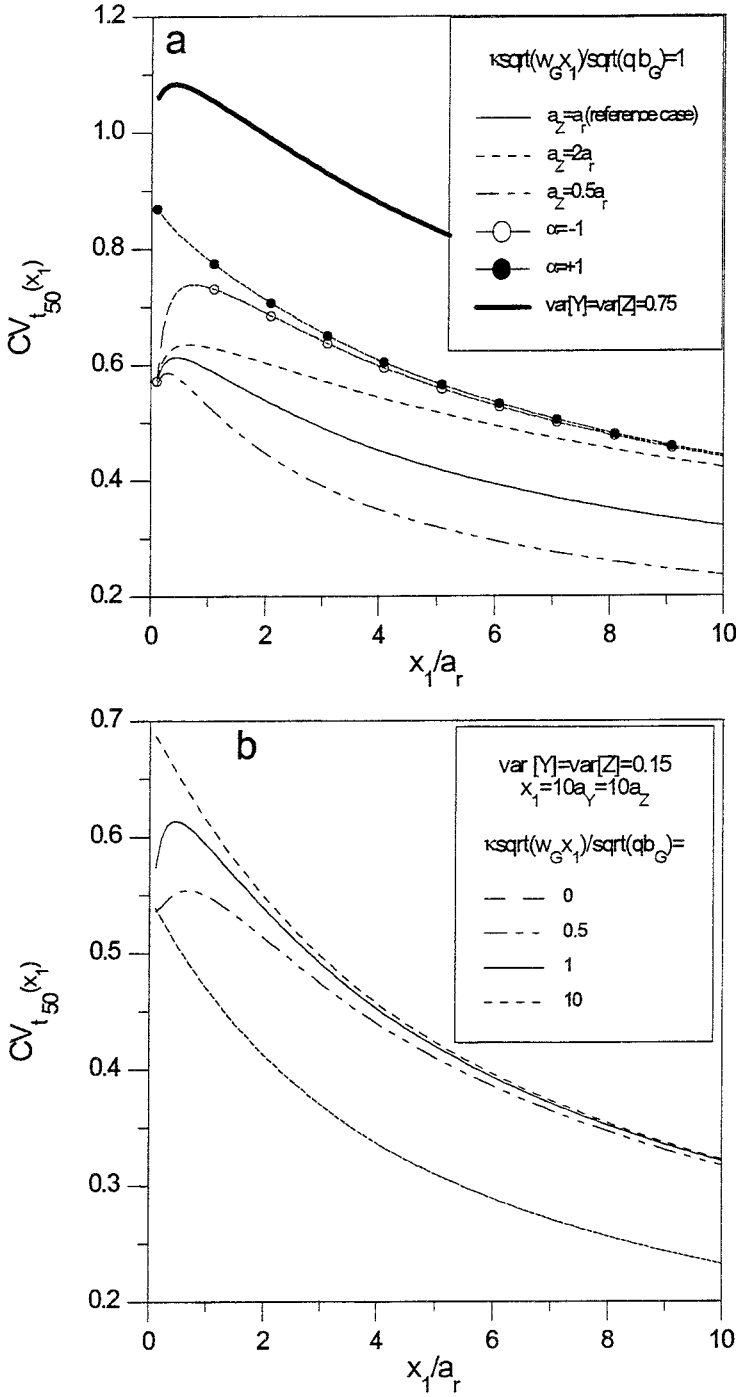

Figure 6.1 *Coefficient of variation for time of 50% accumulated mass (t_{50}) for*
a) different flow path configurations with constant κ, and
b) for the reference flow path with increasing values of κ.

7 Discussion of results and implications

7.1 General formulation

The main result of this report is the identification of the parameter β defined in (23). Using the transformation $\tau = \tau(x_1)$ (for details see e.g. *Cvetkovic and Dagan* (1994)), the results of this report can be shown applicable to a 2D flow in a fracture with variable aperture. The parameter β is then a function of the residence time τ:

$$\beta(\tau) = \int_0^\tau \frac{d\tau'}{b(\tau')} \tag{45}$$

that is used in (21) for evaluating tracer retention in a single fracture. The retention is due to matrix diffusion, and due to sorption in the matrix and on the fracture surface. β is a Lagrangian quantity, integrating the inverse aperture along a flow path. In a general 2D flow situation, the Lagrangian aperture is obtained $b(\tau) = b[\mathbf{X}(\tau)]$ similar to the classical Lagrangian velocity (e.g., *Dagan*, 1984), where $\mathbf{X} = \mathbf{X}(\tau)$ is the advection trajectory. We emphasize that the result (45) implies that different values of β can be obtained for the same value of $\tau \equiv \int_0^\tau d\tau'$ since the aperture distribution may be different along paths yielding the same conservative travel time τ. Only a statistical correlation between β and τ may exist.

The result (21) is general, i.e. independent of the simplified flow path geometry of Section 2.3. The parameter β is a kinematic quantity, however, its dependence on the dynamics of the flow is apparent through $\mathbf{X}(t)$, i.e. $\mathbf{V}(\mathbf{x})$. Models for 2D flow and transport in a fracture plane with spatially variable aperture (where the flow dynamics is explicitly included) can thus be complemented with the result (21) and (45) such that these models also account for spatially variable matrix diffusion. Such complemented models may provide a realistic description of both conservative transport and mass transfer.

Equation (30) and (31) imply that the mass flux statistics can be evaluated as conditioned on a given value of τ with variability in β only. In Figure 7.1 we illustrate the correlation between β and τ for realizations of the kinematic flow path similar to the ones described in Section 4.1. Thus for a fixed τ, a distribution of β is obtained that is evaluated by the conditional pdf $g(\beta \mid \tau)$. Using the Bayesian theorem on conditional probabilities, we can write:

$$h(\beta, \tau; x_1) = g(\beta \mid \tau) g(\tau; x_1) \tag{46}$$

Thus the joint pdf $h(\beta, \tau; x_1)$ that controls the mean and variance of the retarded mass

flux in (28) and (29), can be obtained from the groundwater residence time distribution $g(\tau; x_1)$, and the conditional pdf $g(\beta \mid \tau)$. Figure 7.1 clearly indicates the uncertainty in β for a given τ which is reflected in the uncertainty of the mass flux of Section 5.1. Thus an important topic for future analysis is the computation of the conditional pdf $g(\beta \mid \tau)$ for general flow conditions in a fracture of spatially variable aperture.

7.2 Characterization of retention mechanisms

If surface sorption is negligible ($K_d^f = 0$), we can define one single parameter that controls the retention of tracers in a fracture as

$$\kappa^* \equiv \kappa \beta = \theta \sqrt{D R_m}\, \beta \tag{47}$$

The parameter κ^* summarizes in a simple and transparent manner the influence of different processes on retention. It is a product of two parameters, β and κ. κ is tracer-dependent and is a function of the physical/sorption properties of the rock matrix, but is independent of the flow; κ is assumed measurable in the laboratory from rock samples and for a given tracer. By contrast, β is independent of the tracer, and is entirely dependent on the flow. In the general case, β is a scale-dependent, Lagrangian quantity expressed as a function of fluid (nonreactive tracer) residence time, dependent on the inverse fracture aperture as integrated along a flow path.

Under idealized conditions of tracer transport along a single flow path, the parameter β can be readily determined from a tracer test using the cumulative mass flux, either from a pulse, or a continuous injection, as discussed in Section 6. In particular, from two measured values of t_ϕ, we can compute both τ and β for given κ. For realistic conditions, a tracer test is conducted under stress (pumping) where the cumulative breakthrough would include several flow paths (see e.g. *Selroos et al.*, 1994). In such cases, we need to characterize/estimate the distributions of τ and β rather than single values. This can in principle be done by deconvoluting the cumulative mass flux, and using tracers with different κ values. The correlation between τ and β is of particular interest in this context. The expression for β provides the possibility for establishing the conditional pdf $g(\beta \mid \tau)$ using systematic, relatively straightforward simulations of flow and advective (nonreactive) transport; such simulations would complement the ongoing field investigations within TRUE at Äspö designed for the characterization of retention mechanisms (*Winberg*, 1994).

7.3 Performance assessment

Equations (28) and (29) quantify the mass flux statistics on any scale, in which moments of $h(\beta, \tau; x_1)$ (or of $g(\beta \mid \tau)$ and $g(\tau; x_1)$) need to be appropriately defined. For large scales, the transport is conceptualized as extended flow paths through a 3D network of 2D fractures (Figure 2.3), and (28) and (29) can be used for Performance Assessment (PA). The important feature of the parameter β for PA is its random nature and scale-dependence. Thus the key issue for implementation is how the statistics of β can be extrapolated from scales of a few meters on which measurements/characterization can be made, to scales of few hundreds of meters for PA. A realistic and practical strategy to achieve the scale transition can be made by combining field scale tracer tests (up to say 10m) with numerical simulations of flow and mass transport in fractures and fracture networks.

Of particular interest for PA are the simple expressions for the statistics of the time of mass fraction arrival derived in Section 6. These results can be extended to account for radioactive decay, as well as to incorporate the uncertainty in the time of failure, t_0. Expressions of the type (40) can be derived for these more general conditions, and used for a simple and quick assessment of the impact of a repository on the biosphere for given scenarios. The moments of mass fraction arrival time t_ϕ depend on the (joint)moments of τ and β, of up to fourth order (see (44)). These moments may be difficult (if not impossible) to determine directly from field measurements. However, numerical simulations with currently available models can be used for a statistical estimation of these moments. It is emphasized that β depends only on the flow field, and hence can be simulated using relatively standard simulation codes for nonreactive tracer transport in fractures and fracture networks.

Finally, block scale experiments within TRUE combined with the nonreactive simulations through fracture networks should provide an indication on the upscaling of the parameter β that can be used for PA.

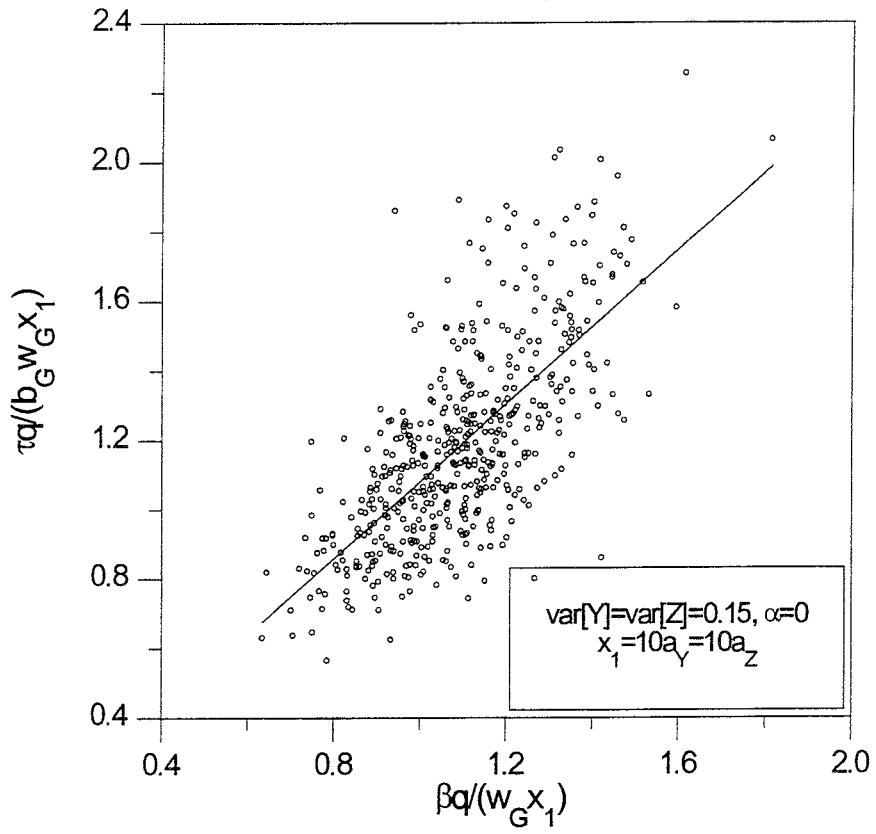

Figure 7.1 *Scattergram visualizing the correlation between β and τ for 500 flow path realizations of the reference case ($\sigma_Y^2 = \sigma_Z^2 = 0.15$, $a_Y = a_Z = a_\tau$, $\alpha = 0$).*

8 Summary

The effect of variability in fracture aperture on advection coupled with matrix diffusion and surface sorption has been analyzed with respect to possible influence on tracer mass flux. An analytical mass flux solution incorporating advection and mass transfer (surface sorption and matrix diffusion combined with matrix sorption) is derived for a single flow path using a Lagrangian approach following the methodology by *Cvetkovic and Dagan* (1994, 1996). The solution is dependent on two parameters: the residence time τ (conservative travel time) and a parameter β. For natural flow paths through heterogeneous media, both β and τ are Lagrangian random variables. Using the two parameters β and τ, an effective half-aperture is defined, a "mass balance aperture" in the terminology of *Tsang* (1992). The analytical solution is applicable for general two-dimensional flow in fracture planes with spatially variable aperture.

The analytical result is applied using a kinematic prototype of a flow path that extends the simplified model proposed by O. Olsson in *Olsson et al.* (1995). For the simplified flow path geometry, the parameter β is equal to the surface area in contact with the rock matrix, normalized by the fluid volumetric flux. The flow path width and aperture are spatially variable and defined through random space functions. For flow paths with a constant width and only varying aperture, it is shown that the parameter β is a constant value; for this case the tracer flux moments are based on only one random variable, i.e. τ.

Based on the underlying random space functions defining prototype flow paths, the first two moments of β and τ (expected values, variances and covariance) are derived analytically in an exact manner. The results are expressed in integral form and are evaluated through quadrature. The assumption of width and aperture correlation models with finite correlation ranges has been assessed through an alternative use of self-similar correlation models with infinite correlation ranges. The results using self-similar correlation models show wider β and τ distributions, i.e. larger second moments of β and τ for given aperture and width variability (Appendix, 9.2). The results based on the self-similar model may provide indications on the β and τ statistics for more complex problems.

Solute flux moments have been derived hypothesizing probability density functions for the two random variables β and τ. The effect of variability in β and the residence time, τ, on the mass flux is assessed by evaluating the mass flux moments using univariate pdfs for β and τ, respectively. It is shown that the quantitative effect of variability in

β is considerably larger on the mass flux moments than the corresponding variability in τ. Furthermore, it is shown that the qualitative effect of variability in β and τ on the mass flux moments also differ; variability in β results in an expected mass flux with a pronounced peak larger than the peak of the corresponding deterministic mass flux, whereas variability in τ results in a temporally more spread mass flux with a lower peak than that of the deterministic mass flux. However, for the analyzed cases with low variability ($\sigma_Y^2 = \sigma_Z^2 = 0.15$), the difference between the expected and deterministic mass fluxes is minor. The different effects of surface sorption, and matrix diffusion combined with sorption, has been investigated. Surface sorption primarily implies a mere translation (delay) of the breakthrough curve, whereas matrix diffusion results in a breakthrough curve with pronounced tailing.

Moments of the time of arrival of a particular mass fraction, t_ϕ, have also been derived. These moments are obtained directly from the moments of β and τ (up to fourth order) without hypothesizing a probability density function. It is shown that β has a stronger influence on the moments of t_ϕ than τ has. Furthermore, a non-zero sorption parameter κ implies larger prediction uncertainties than in the nonreactive case.

The presented results are valid for a single flow path, i.e. the expected tracer flux is the mean flux from an ensemble of flow paths following the same width and aperture variability, and the flux variance expresses the mass flux prediction uncertainty. However, the results (28) and (30) can also be used for the case where multiple flow paths contribute to the resulting mass flux. For this case the residence time pdf is the real measured water residence time distribution, i.e. fully ergodic conditions prevail (e.g. *Dagan*, 1990, 1991; *Selroos and Cvetkovic*, 1994; *Selroos*, 1995). Correspondingly, the pdf of β represents all β-values of the ensemble of contributing flow paths. The expected tracer flux is then the flux which would be measured, and the flux variance is equal to zero.

The obtained results can be used for characterization of matrix diffusion under field conditions. Specifically if only one flow path is investigated, the conservative travel time, τ, in combination with t_ϕ and κ provides a possibility to estimate β. Alternatively, two values of t_ϕ in combination with κ provides the possibility to estimate both β and τ. For experimental conditions where several flow paths are sampled, an effective β-value can be estimated based on the conservative residence time distribution (conservative breakthrough), on κ and on the reactive breakthrough. Using the effective β-value, predictions can be made for other tracers (different κ-values) and other flow rates (different q-values) as long as all tracers follow the same flow paths.

If a prediction of a reactive breakthrough is to be made for another flow path based on the knowledge of κ and moments of τ, the moments of β and correlation between β and τ have to be assumed. Thus it is of interest to analyze the correlation pattern for various experimental conditions in numerical simulations of flow and mass transport.

The main relevance of the obtained results for Performance Assessment is the additional prediction uncertainty implied by the random nature of β. The results show that the statistics of β more strongly affect the predictions of reactive travel times than the statistics of the conservative travel time τ does; thus the assumption of an effective β-value in Performance Assessment studies may imply unconservative predictions. One of the main issues to be addressed with regard to Performance Assessment is if correlation patterns obtained between β and τ at experimental scales are valid or can be extrapolated to the larger scales that usually are of interest in safety assessment studies. However, small scale (5m) and block scale (50m) field experiments in combination with numerical simulations may provide indications on possible methods for scale transitions.

9 Appendix

9.1 Analytical solution for the mass flux

The solution for γ is obtained by taking the Laplace transform of (15), (16), and (19). A system of equations in the Laplace domain is obtained as

$$R_f(x_1)\widehat{S}p + \frac{d\widehat{S}}{dx_1} = \frac{\theta D}{b(x_1)}\frac{d\widehat{N^*}}{dx_3} \qquad \text{for} \qquad x_3 = 0, \qquad x_1 > 0 \tag{48}$$

$$\frac{d^2\widehat{N^*}}{dx_3^2} - p'^2\widehat{N^*} = 0 \qquad \text{for} \qquad x_3 > 0 \quad , \quad x_1 > 0 \tag{49}$$

$$\widehat{S} = \widehat{N^*} \qquad \text{for} \qquad x_3 = 0 \tag{50}$$

where the circumflex denotes the Laplace transform, p is the Laplace transform variable, and $p' \equiv (pR_m/D)^{1/2}$. The solution of (49) is $\widehat{N^*} = \widehat{S}\exp(-p'x_3)$ whereby (48) with (50) reduces to

$$\frac{d\widehat{S}}{dx_1} = -\left[\frac{R_f(x_1)}{V_1(x_1)}p + \frac{\kappa'}{V_1(x_1)b(x_1)}p'\right]\widehat{S} \tag{51}$$

where $\kappa' = \theta D$.

The transformed boundary and initial conditions are

$$\widehat{S} = \rho_0 \qquad \text{for} \qquad x_1 = 0$$

$$\widehat{N^*} \qquad \text{finite as} \qquad x_3 \to \infty \tag{52}$$

$$\widehat{N^*} \quad \text{and} \quad \widehat{S} \quad \text{finite as} \quad x_1 \to \infty$$

Integration of (51) with (52) yields

$$\widehat{S} = \rho_0 \exp\left[-p(\tau + \beta K_d^f)\right] \exp\left(-\kappa'\beta p'\right) \tag{53}$$

where β is given in (24) and τ is given in (26). Inversion of (53) yields (*Carslaw and Jaeger*, 1959)

$$S(t,\tau) = \rho_0\,\gamma(t,\tau;\beta) \tag{54}$$

where γ is given in (21).

9.2 Analytical moments of β and τ

Inserting the second expression (32) into the definition of β (24) yields

$$\beta = \frac{w_G}{q} \int_0^{x_1} \exp\left[\alpha Y(x) + Z(x)\right] dx \tag{55}$$

Recognizing that Y and Z are normally distributed and uncorrelated, the first two moments of β are obtained using the standard relationship between moments of normally and lognormally distributed variables. Thus the expected value of β in (36) is obtained as

$$< \beta(x_1) > \equiv \overline{\beta}(x_1) = \frac{w_G x_1}{q} \exp\left[\alpha^2 \frac{\sigma_Y^2}{2} + \frac{\sigma_Z^2}{2}\right] \tag{56}$$

and the variance of β in (37) as

$$\begin{aligned} \sigma_\beta^2(x_1) &= \frac{2w_G^2}{q^2} \exp\left[\alpha^2 \sigma_Y^2 + \sigma_Z^2\right] \\ &\cdot \int_0^{x_1} (x_1 - x) \left[\exp\left[\alpha^2 C_Y(x) + C_Z(x)\right] - 1\right] dx \end{aligned} \tag{57}$$

where $x = |x_1' - x_1''|$.

The residence time moments are derived analogously to the moments of β above. Inserting the expressions for b and w in (32) into the expression for the residence time (26) yields

$$\tau(x_1) = \frac{b_G w_G}{q} \int_0^{x_1} \exp\left[(\alpha + 1) Y(x) + Z(x)\right] dx \tag{58}$$

Using the relationship between moments of normally and lognormally distributed variables, the first moment of τ in (38) is obtained as

$$< \tau(x_1) > \equiv \overline{\tau}(x_1) = \frac{b_G w_G x_1}{q} \exp\left[\frac{(\alpha + 1)^2 \sigma_Y^2}{2} + \frac{\sigma_Z^2}{2}\right] \tag{59}$$

and the variance in (39) as

$$\begin{aligned} \sigma_\tau^2(x_1) &= \frac{2b_G^2 w_G^2}{q^2} \exp\left[(\alpha + 1)^2 \sigma_Y^2 + \sigma_Z^2\right] \\ &\cdot \int_0^{x_1} (x_1 - x) \left[\exp\left[(\alpha + 1)^2 C_Y(x) + C_Z(x)\right] - 1\right] dx \end{aligned} \tag{60}$$

where $x = |x_1' - x_1''|$.

The coefficient of correlation between β and τ is obtained as

$$\rho_{\beta\tau}(x_1) \equiv \sigma_{\beta\tau}(x_1) / [\sigma_\beta(x_1)\sigma_\tau(x_1)] = \frac{\exp[\mathrm{cov}[B(x_1), T(x_1)]] - 1}{\sqrt{\exp(\sigma_B^2) - 1}\sqrt{\exp(\sigma_T^2) - 1}} \tag{61}$$

where $B(x_1) = \int_0^{x_1} [\alpha Y(x) + Z(x)]\, dx$ and $T(x_1) = \int_0^{x_1} [(\alpha+1) Y(x) + Z(x)]\, dx$. The covariance between B and T in (61) is obtained as

$$\begin{aligned}
\mathrm{cov}[B(x_1), T(x_1)] &= \int_0^{x_1}\int_0^{x_1} < B(x')T(x'') > dx'dx'' \\
&\quad - \int_0^{x_1} < B(x') > dx' \int_0^{x_1} < T(x') > dx' \\
&= \int_0^{x_1}\int_0^{x_1} < [\alpha Y(x') + Z(x')][(\alpha+1) Y(x'') + Z(x'')] > dx'dx'' \\
&= 2\int_0^{x_1} (x_1 - x)[\alpha(\alpha+1) C_Y(x) + C_Z(x)]\, dx
\end{aligned} \tag{62}$$

where $x = |x_1' - x_1''|$. The variance of B in (61) is obtained as

$$\begin{aligned}
\sigma_B^2(x_1) &= \int_0^{x_1}\int_0^{x_1} < B(x')B(x'') > dx'dx'' - \left[\int_0^{x_1} < B(x') > dx'\right]^2 \\
&= \int_0^{x_1}\int_0^{x_1} < [\alpha Y(x') + Z(x')][\alpha Y(x'') + Z(x'')] > dx'dx'' \\
&= 2\int_0^{x_1} (x_1 - x)\left[\alpha^2 C_Y(x) + C_Z(x)\right] dx
\end{aligned} \tag{63}$$

where $x = |x_1' - x_1''|$. The variance of T is obtained correspondingly to (63) with the constant α^2 in front of C_Y replaced by $(\alpha+1)^2$.

Flow paths with finite correlation length

In Figure A1 the resulting β- and τ-ensemble moments are presented for the same flow path statistics that were shown in Figure 4.2 as individual realizations. In Figure A1a the coefficient of variation $\mathrm{CV}_\beta(x_1) = \sigma_\beta(x_1)/\overline{\beta}(x_1)$ is presented. In Figure A1b the corresponding coefficient of variation $\mathrm{CV}_\tau(x_1)$ is presented. In Figure A1c the coefficient of correlation between β and τ, $\rho_{\beta\tau}(x_1)$, is presented. Depending on the spatial correlation model adopted, either (33) or (34) is used in the evaluation of the variances (57) and (60).

For the reference case it is assumed that the aperture and width statistics are identical. The variances are $\sigma_Y^2 = \sigma_Z^2 = 0.15$, the correlation distances of the exponential

spatial correlation models are $a_Y = a_Z = a_\tau$, and the correlation parameter is $\alpha = 0$. It is observed in both Figure A1a and A1b that the CVs decrease with distance; since the expected values are linear functions of distance, the standard deviations grow non-linearly with distance with an exponent less than one. The coefficient of correlation between β and τ is independent of distance (Figure A1c).

Doubling the width correlation distance a_Z yields higher CVs for both β and τ. With a longer correlation distance, less of the ensemble statistics is embedded in a single flow channel, and hence the flow channel integrated entities are more uncertain. Furthermore, $\rho_{\beta\tau}$ increases with distance for the case with an increased correlation distance a_Z (Figure A1c). With reducing a_Z-values, opposite features are observed.

When the width and aperture are correlated through the parameter α, a larger CV_β is obtained. The effect of the introduced dependence of the width on the RSF Y is thus a larger uncertainty in β. This follows from the fact that less of the ensemble statistics of β is embedded in a single flow path realization when the width is a function of two independent, rather than one, RSFs and thus exhibits more variability. The residence time variability is reduced for $\alpha = -1$ and increased for $\alpha = +1$ (Figure A1b). The negative α-value, implying relatively larger widths for smaller apertures and vice versa, tends to yield residence times of the same magnitude in different realizations and thus results in a smaller residence time uncertainty. A positive value has an opposite effect on the residence time variability; furthermore, $\rho_{\beta\tau}$ increases dramatically for the positive α-value (Figure A1c). The latter phenomenon is rather intuitive; when both the width and aperture show large values at the same locations along the flow path, β and τ show stronger correlation since both are dependent on both width and aperture. For $\alpha = -1$, the same correlation between β and τ is obtained as in the reference case.

Increasing the variance of Z to $\sigma_Z^2 = 0.75$ results in larger CV_β using both the exponential and Gaussian spatial correlation models for Z (for the Gaussian model the correlation distance is $a_Z = \sqrt{3}a_\tau$). Thus, with more variability along the channel, the uncertainty in the parameter β increases. For short distances ($x_1 < 3a_\tau$), the exponential and Gaussian models yield CV_β with different shapes. Moreover, the magnitude of the Gaussian CV_β is larger at all distances. These features follow from the difference in spatial correlation functions as seen in Figure 4.1. Similar effects are seen for $\mathrm{CV}\tau$ when Y is given by the same statistics as Z. However, the coefficient of correlation, $\rho_{\beta\tau}$, is not affected by the increased variances for either the exponential or Gaussian models, but is identical to the reference case.

When the variability is increased by assuming either $\sigma_Y^2 = 0.75$ and $\sigma_Z^2 = 0.15$,

or by assuming $\sigma_Y^2 = 0.15$ and $\sigma_Z^2 = 0.75$, a CV_τ with intermediate magnitude is observed compared to the cases where both variances are given by $\sigma_Y^2 = \sigma_Z^2 = 0.15$ or by $\sigma_Y^2 = \sigma_Z^2 = 0.75$. This is shown in Figure A1b for the exponential model. Variability in aperture and width thus have the same quantitative effect on the residence time prediction uncertainty; this follows directly from the residence time definition (26) where τ is given as linearly dependent on both width and aperture. The effect of different aperture and width variability on the correlation coefficient is shown in Figure A1c; a reduction in either σ_Y^2 or σ_Z^2 results in a smaller but spatially constant $\rho_{\beta\tau}$.

In these illustration examples, a number of different parameter combinations have been analyzed. Other combinations could also be constructed. A change in the half-aperture correlation distance a_Y will leave the β-distribution unchanged if $\alpha = 0$. An increase in a_Y results in a larger residence time variance and in a lower correlation between β and τ if $\alpha = 0$; the opposite is true for a decrease in a_Y.

Self-similar flow paths

The spatial correlation models adopted above for the half-aperture and width, i.e. the exponential and Gaussian models, are both characterized by finite correlation ranges. This implies that the width at two locations separated by a distance significantly larger than the correlation range exhibits zero correlation. However, one could hypothesize that both the flow path aperture and width in fractures have extended correlation structures and are characterized by self-similarity.

Fractional Gaussian noise (fGn) is characterized by a spatial covariance function with self-similar properties (*Mandelbrot and Van Ness*, 1968; *Cvetkovic*, 1991)

$$C(r) = \frac{\sigma^2}{2}\left(\left|\frac{r}{\varepsilon}+1\right|^{2H} - 2\left|\frac{r}{\varepsilon}\right|^{2H} + \left|\frac{r}{\varepsilon}-1\right|^{2H}\right) \tag{64}$$

where H is the Hurst exponent, and ε is a smoothing parameter. For large values of r/ε, (64) is proportional to r and does not dependent on ε. We shall for simplicity assume $\varepsilon = 1$. In Figure A2 the correlation function $C(r)/C(0) = C(r)/\sigma^2$ is presented for different values of the Hurst exponent H. In the limit $H = 1$ perfect correlation exists between all values, and $C(r) = \sigma^2$ for all r. Applied to the flow path width and aperture, this would imply a flow path with constant, but uncertain, width and aperture. Thus a uniform, rectangular channel model is obtained (e.g., *Neuzil et al.*, 1981; *Neretnieks*, 1982). For decreasing values of H, correlation functions with smaller magnitude of correlation are obtained, although the correlation ranges are still infinite.

In Figure A3a and A3b the resulting CV_β and CV_τ are shown for a set of different parameter combinations where both the half-aperture and width spatial correlation functions are given by the fGn-model. The second moments of β and τ have been evaluated analytically using (64) in (57) and (60). The main observation in Figure A3a and A3b is that the CVs do not decay with distance. Furthermore, the CVs are insensitive to the exponent H in the range $0.5 < H < 1$. For a value $H = 0.2$, only small decreases in the CVs are obtained. This is explained by the fact that the spatial correlation functions never reach zero even for small values of H.

An implication of the results shown in Figure A3a and A3b is that the individual realizations contain less of the ensemble statistics as the correlation distance is infinite. In the limit $H = 1$, each realization contains only one width value and one aperture value, thus resulting in large ensemble uncertainty of β and τ. Since the CVs of the fGn model do not depend strongly on distance, the variances of β and τ are larger than the corresponding variances for the exponential and Gaussian correlation models in Figure A1a and A1b for increasing x_1-values. It is observed that $CV_\beta(x_1 = 0) = 0.4$ in Figure A1a and A3a when $\sigma_Z^2 = 0.15$ and $\alpha = 0$, i.e. the same CV as that of the assumed underlying flow path variability ($CV_w = \sqrt{\exp(0.15) - 1} = 0.4$).

The effects of the parameter α and variances σ_Y^2 and σ_Z^2 on CV_β and CV_τ are also exemplified in Figure A3a and A3b. The same magnitude changes as in Figure A1a and A1b are observed; however, in Figure A3a and A3b the CVs do not decay with distance. The correlation between β and τ is independent of distance for the cases considered in Figure A3a and A3b; furthermore, $\alpha = 1$ implies an increased correlation between β and τ.

9.3 Moments of β and τ obtained by first-order expansion

A first-order perturbation (expansion) approach resulting in closed-form solutions of the variances and higher order moments is conducted for cases with small variability in Y and Z ($\sigma^2 < 1$). The closed-form solutions of the variances are primarily of interest in that they are based on approximations frequently used for more complex systems where exact solutions are not available. For the simplified flow geometry considered in the current illustration example, the effect of the adopted approximations may be assessed quantitatively by comparing the expansion results with the exact analytical solutions. Furthermore, exact solutions are not available for the higher order moments used in Section 6; the accuracy of the variances provides an indication of the robustness of the higher order moments.

The second moment of β is obtained by applying the expectation operator on the squared fluctuations of β, $\sigma_\beta^2(x_1) =< \beta'(x_1)\beta'(x_1) >$ where $\beta' = \beta - \overline{\beta}$. Using a first-order expansion analysis, the width is approximated as $w(x_1) = w_G \exp[\alpha Y(x_1) + Z(x_1)]$ $\approx w_G[1 + Z(x_1) + \alpha Y(x_1) + \alpha Y(x_1) Z(x_1)]$. When evaluating the fluctuation β', the mean value $\overline{\beta} = w_G x_1/q$ is used. Developing the expression for β' using the expanded expression for w, and applying the expectation operator on the squared expression yields

$$\begin{aligned}\sigma_\beta^2(x_1) &= \frac{w_G^2}{q^2}\int_0^{x_1}\int_0^{x_1} < \alpha^2 Y(x')Y(x'')\,dx'dx'' + Z(x')Z(x'') > dx'dx'' \\ &= \frac{2w_G^2}{q^2}\int_0^{x_1}(x_1 - x)\,\alpha^2 C_Y(x) + (x_1 - x)\,C_Z(x)\,dx\end{aligned} \tag{65}$$

where C_Z and C_Y are the covariance functions for Z and Y, respectively, and $x = |x_1' - x_1''|$. Inserting the exponential covariance expression (33) for both Z and Y into (65) yields the second moment of β

$$\begin{aligned}\sigma_\beta^2(x_1) &= \frac{2w_G^2}{q^2}\left[\alpha^2\sigma_Y^2\int_0^{x_1}(x_1 - x)\exp\left(\frac{-x}{a_Y}\right)dx + \sigma_Z^2\int_0^{x_1}(x_1 - x)\exp\left(\frac{-x}{a_z}\right)dx\right] \\ &= \frac{2w_G^2}{q^2}\left[\alpha^2\sigma_Y^2\left[x_1 a_Y + a_Y^2\left(\exp\left(\frac{-x_1}{a_Y}\right) - 1\right)\right] + \sigma_Z^2\left[x_1 a_Z + a_Z^2\left(\exp\left(\frac{-x_1}{a_Z}\right) - 1\right)\right]\right]\end{aligned} \tag{66}$$

The closed-form expression for the variance of τ is obtained by a first-order approximation of the product between the half-aperture and width according to

$$\begin{aligned}b(x_1)\,w(x_1) &= b_G w_G \exp[Y(x_1) + \alpha Y(x_1) + Z(x_1)] \\ &\approx b_G w_G[1 + Z(x_1) + (\alpha + 1)Y(x_1) + (\alpha + 1)Y(x_1)Z(x_1)]\end{aligned}$$

Applying the expectation operator on the square of the fluctuations $\tau' = \tau - \overline{\tau}$, where $\overline{\tau} = b_G w_G x_1/q$, yields

$$\sigma_\tau^2(x_1) = \frac{w_G^2 b_G^2}{q^2}\int_0^{x_1}\int_0^{x_1} < \left(\alpha^2 + 2\alpha + 1\right)Y(x')Y(x'') + Z(x')Z(x'') > dx'dx'' \tag{67}$$

It is observed that the only difference between (67) and the first expression in (65) is the constant terms in front of $Y(x')Y(x'')$ and $Z(x')Z(x'')$; consequently the rest of the development of the second moment of τ is identical to the development of the second moment of β above. The result is finally obtained as

$$\sigma_\tau^2(x_1) = \frac{2b_G^2 w_G^2}{q^2}\left[(\alpha^2+2\alpha+1)\,\sigma_Y^2\left[x_1 a_Y + a_Y^2\left(\exp\left(\frac{-x_1}{a_Y}\right)-1\right)\right]\right.$$
$$\left. + \sigma_Z^2\left[x_1 a_Z + a_Z^2\left(\exp\left(\frac{-x_1}{a_Z}\right)-1\right)\right]\right] \tag{68}$$

In order to evaluate $\sigma_{t_\phi}^2$ in (44), the fourth-order moment $\overline{\beta^4}$ and the third-order cross moment $\overline{\beta^2\tau}$ have to be computed. Using the same approximation for the width as in the development of σ_β^2, the fourth-order moment is obtained using similar steps as above as

$$\overline{\beta^4}(x_1) = \left(\frac{w_G x_1}{q}\right)^4 + 6\left(\frac{w_G}{q}\right)^4 x_1^2 \int_0^{x_1}\int_0^{x_1} \alpha^2 C_Y(x'-x'') + C_Z(x'-x'')\,dx'dx''$$
$$+3\left(\frac{w_G}{q}\right)^4\left[\int_0^{x_1}\int_0^{x_1}\alpha^2 C_Y(x'-x'')\,dx'dx''\right]^2 + 3\left(\frac{w_G}{q}\right)^4\left[\int_0^{x_1}\int_0^{x_1} C_Z(x'-x'')\,dx'dx''\right]^2 \tag{69}$$

where the double integrals over C_Y and C_Z are evaluated as in (65) and (66).

The third-order cross moment is obtained as

$$\overline{\beta^2\tau}(x_1) = \left(\frac{b_G w_G x_1}{q}\right)^3 + 3\left(\frac{b_G w_G}{q}\right)^3 x_1 \int_0^{x_1}\int_0^{x_1} \alpha(\alpha+1)\,C_Y(x'-x'') + C_Z(x'-x'')\,dx'dx'' \tag{70}$$

where the double integrals over C_Y and C_Z are evaluated as in (65) and (66).

In Figure A4a an assessment of the validity of the first-order expansion results is performed. A comparison between the first moment of β given by the exact analytical result (56) and the expansion result $\overline{\beta} = w_G x_1/q$ is presented in Figure A4a. In Figure A4b a comparison between the exact analytical second moment σ_β^2 in (57) and the corresponding expansion result (66) is made. The effect of different variability in Z on the moments is analyzed; for all cases $\alpha = 0$.

The linear relationship between $\overline{\beta}$ and x_1 is clearly observed in Figure A4a. For increasing σ_Z^2 the slope of the analytical result becomes steeper. However, the expansion result is independent of the variance of Z. Thus the error in the expansion result increases with increasing σ_Z^2. With $\alpha \neq 0$ the error in the expansion result would be even greater.

The variance of β also increases with distance (Figure A4b). The expansion result incorporates the feature of larger variances in β for increasing variability in Z. However, it is clearly observed that the expansion result is valid only for $\sigma_Z^2 \ll 1$; the error increase

of the expansion result is dramatic when increasing σ_Z^2 from 0.15 to 0.75. Similarly to the first moment, the error in the second moment increases when $\alpha \neq 0$.

The first-order expansion moments of τ behave similarly to the ones of β. However, since the variance of τ is larger than that of β if $\alpha > -1/2$, the error in the expansion approximation will also be larger for τ than for β for these cases. The accuracy of the higher-order moments of β and the cross-moments between β and τ can not be assessed directly since exact analytical solutions are not available. However, the comparison between the exact analytical and expansion results for the first two moments provide indications on the accuracy of the adopted simplifications for the higher order moments.

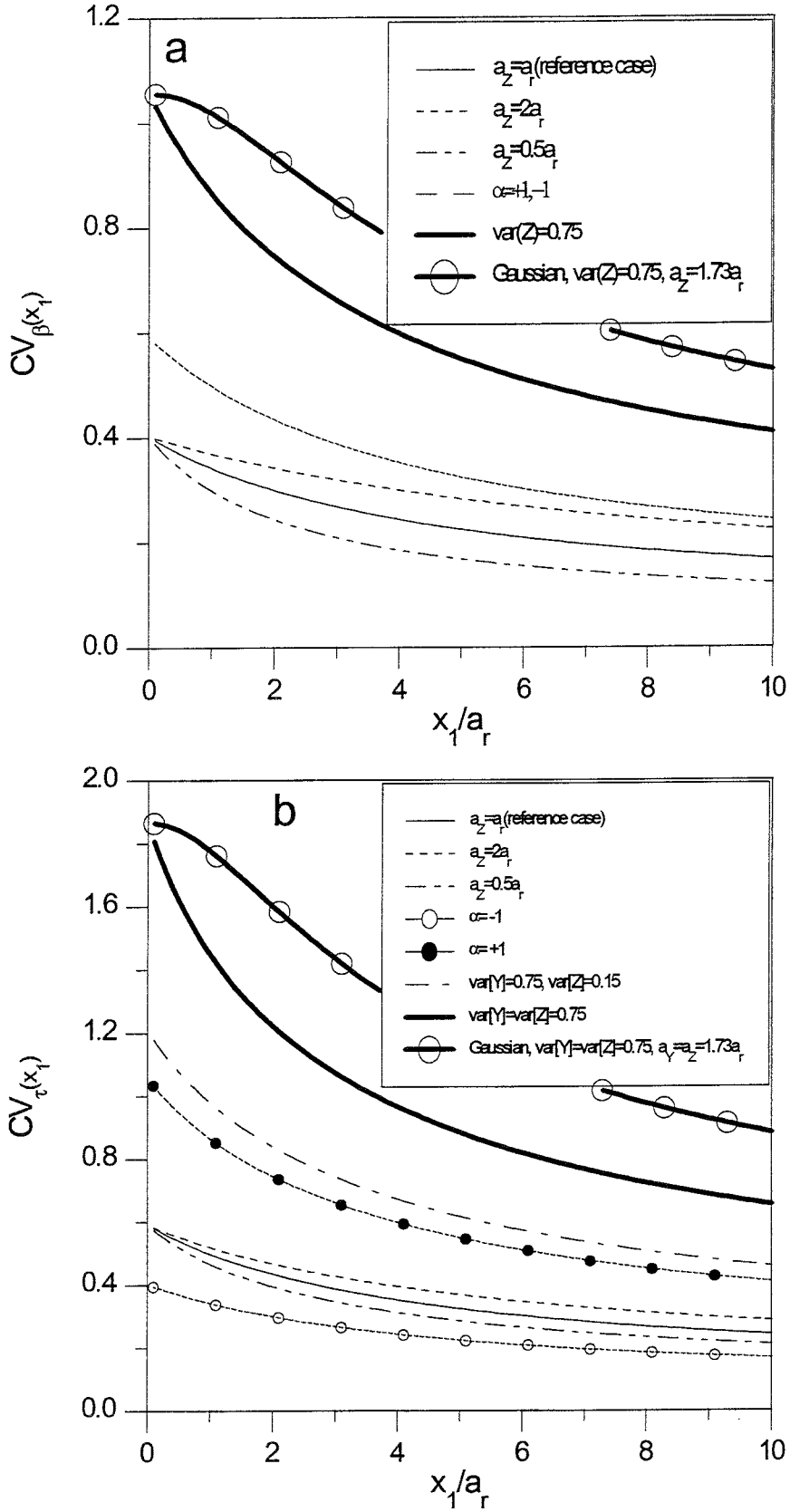

Figure A1 *Coefficient of variation for different flow path configurations for a) parameter β and b) residence time τ.*

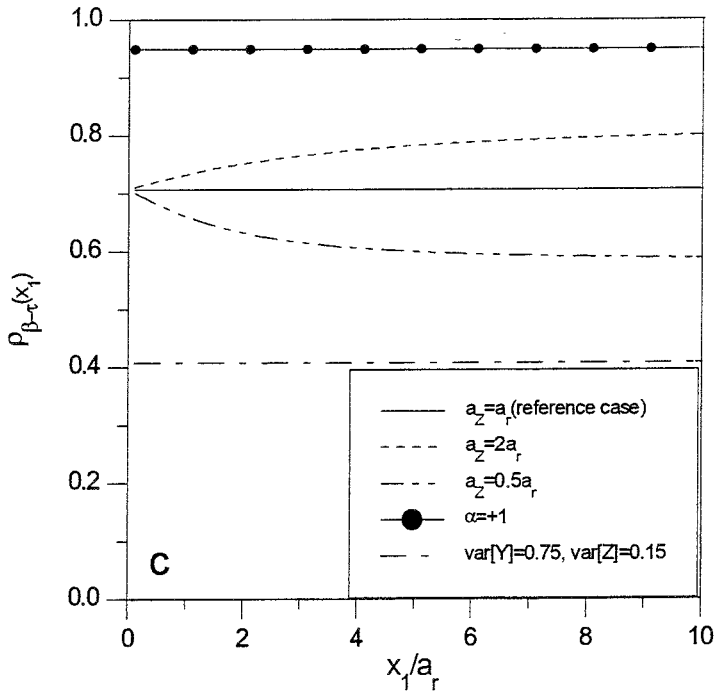

Figure A1 *c) Correlation coefficient between β and τ for different flow path configurations as a function of distance.*

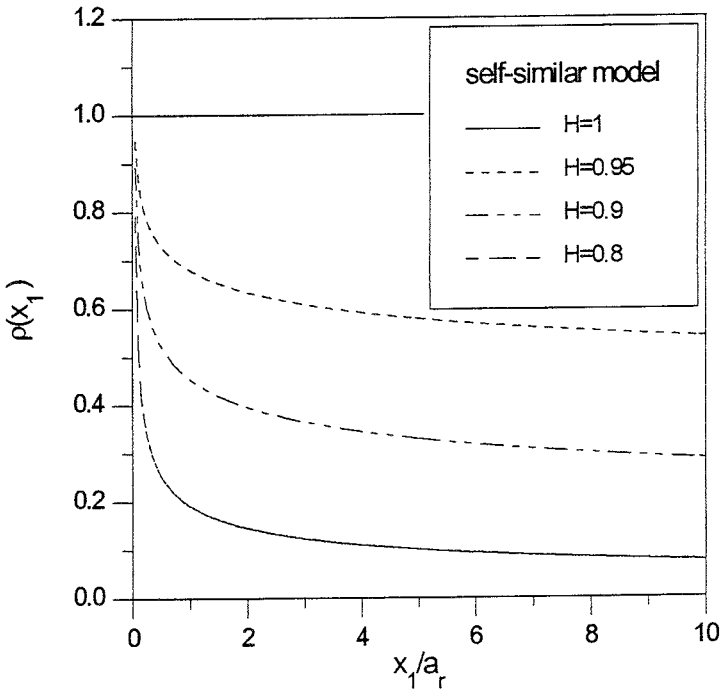

Figure A2 *Correlation function for Self-similar model with different Hurst exponents.*

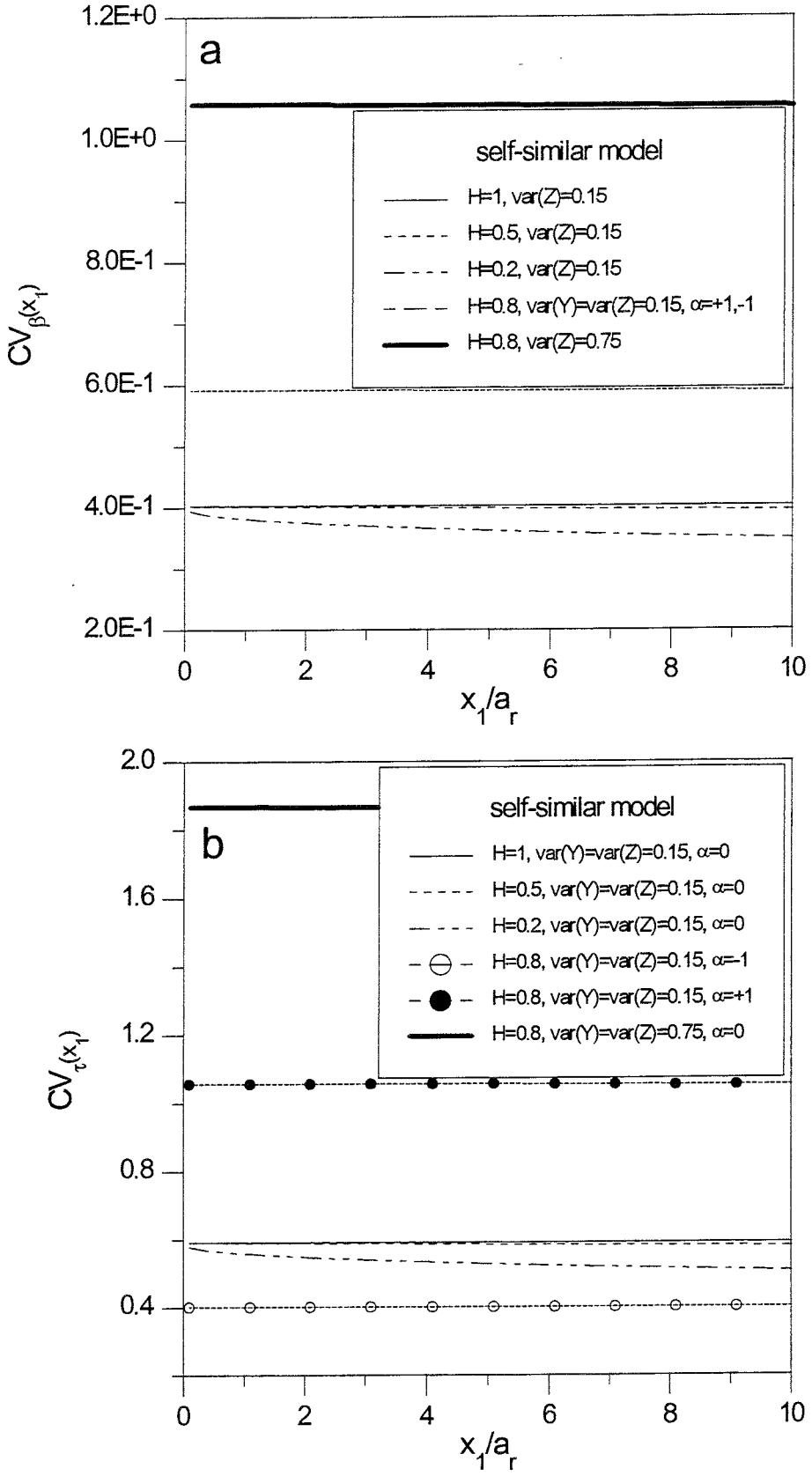

Figure A3 *Coefficient of variation for a) parameter β, and b) residence time τ for flow paths based on the Self-similar spatial correlation model.*

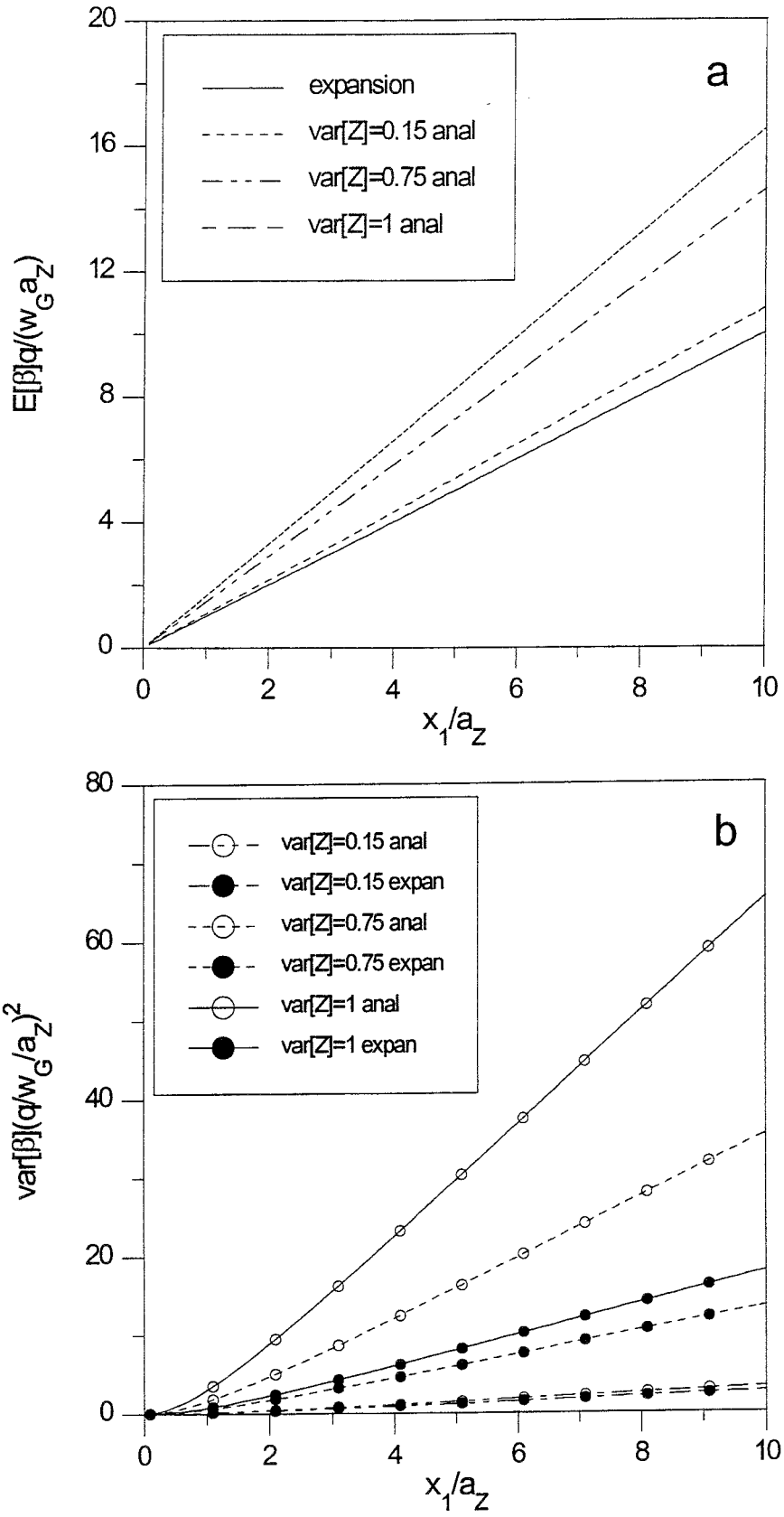

Figure A4 *Comparison between exact analytical solution and approximate expansion solution for a) first moment of β, and b) second moment of β for increasing values of σ_Z^2 with $\alpha = 0$.*

10 References

Abelin, H., I. Neretnieks, S. Tunbrant, and L. Moreno, Final report of the migration in a single fracture - experimental results and evaluation, International OECD/NEA Stripa Project, SKB (Swedish Nuclear Fuel and Waste Management Company) Stripa Technical Report TR 85-03, Stockholm, Sweden, 1985.

Carslaw, H. S. and J. C. Jaeger, *Conduction of heat in solids*, Oxford University Press, New York, 1959.

Cvetkovic, V., Mass arrival of reactive solute in single fractures, *Water Resour. Res.*, 27, 177-183, 1991.

Cvetkovic, V., G. Dagan, and A. M. Shapiro, An exact solution of solute transport by one-dimensional random velocity fields, *Stoch. Hydrology and Hydraulics*, 5, 45-54, 1991.

Cvetkovic, V., and G. Dagan, Tranport of kinetically sorbing solute by steady random velocity in heterogeneous porous formations, *J. Fluid Mech.*, 265, 189-215, 1994.

Cvetkovic, V., and G. Dagan, Reactive transport and immiscible flow in geological media, II. Applications, *Proc. R. Soc. Lond.* A, 452, 303-328, 1996.

Cvetkovic, V., and G. Dagan, Lagrangian modeling of reactive solute transport in aquifers with spatially variable flow and transport parameters, 1 Theory, in prep.

Dagan, G., Solute transport in heterogeneous formations, *J. Fluid Mech.*, 145, 151-177, 1984.

Dagan, G., Transport in heterogeneous porous formations: Spatial moments, ergodicity and effective dispersion, *Water Resour. Res.*, 26, 1281-1290, 1990.

Dagan, G., Dispersion of a passive solute in non-ergodic transport by steady velocity fields in heterogeneous formations, *J. Fluid Mech.*, 233, 197-210, 1991.

Dagan, G., and V. Cvetkovic, Reactive transport and immiscible flow in geological media, I. General theory, *Proc. R. Soc. Lond.* A, 452, 285-301, 1996.

Frick, U. et al., The radionuclide migration experiment - overview of investigations1985-1990, NAGRA (National Cooperative for the Disposal of Radioactive Waste) Technical Report 91-04, Wettingen, Switzerland, 1992.

Hakami, E., and E. Larsson, Aperture measurements and flow experiments on a single natural fracture, *Int. J. of Rock Mechanics and Mining Sciences & Geomech. Abstr.*, in press.

Lee, H. S., L. Moreno, and I. Neretnieks, Some properties of a channel network model, Proceedings from Geoval-1990, Symposium on Validation of Geosphere Flow and Transport Models, Organised by the Swedish Nuclear Power Inspectorate (SKI) and the OECD Nuclear Energy Agency, Stockholm, 14-17 May 1990.

Mandelbrot, B. B., and J. W. Van Ness, Fractional brownian motions, fractional noises and applications, SIAM Rev., 10, 422-437,1968.

Moreno, L., Y. W. Tsang, C. F. Tsang, F. V. Hale, and I. Neretnieks, Flow and tracer transport in a single fracture: A stochastic model and its relation to some field observations, *Water Resour. Res.*, 24, 2033-2048, 1988.

Moreno, L., and I. Neretnieks, Flow and nuclide transport in fractured media: The importance of flow-wetted surface for radionuclide migration, *J. Contaminant Hydr.*, 13, 49-71, 1993.

Moreno, L., B. Gylling, and I. Neretnieks, Solute transport in fractured media - The important mechanisms for performance assessment, SKB (Swedish Nuclear Fuel and Waste Management Company) Technical Report TR 95-11, Stockholm, Sweden, 1995.

Neretnieks, I., Diffusion in the rock matrix: An important factor in radionuclide retardation?, *J. Geophysical Res.*, 85, 4379-4397, 1980.

Neretnieks, I., T. Eriksen, and P. Tähtinen, Tracer movement in a single fissure in granitic rock: Some experimental results and their interpretation, *Water Resour. Res.*, 18, 849-858, 1982.

Neretnieks, I., Solute transport in fractured rock - applications to radionuclide waste repositories, in *Flow and contaminant transport in fractured rock*, Academic Press, Inc., 1993.

Neuzil, C. E., and J. V. Tracy, Flow through fractures, *Water Resour. Res.*, 17, 191-199, 1981.

Olsson, O., I. Neretnieks, and V. Cvetkovic, Delibrations on radionuclide transport and rationale for tracer transport experiments to be performed at Äspö - a selection of papers, SKB (Swedish Nuclear Fuel and Waste Management Company) Progress Report PR 25-95-01, Stockholm, Sweden, 1995.

Selroos, J. O., Temporal moments for nonergodic solute transport in heterogeneous aquifers, *Water Resour. Res.*, 31, 1705-1712, 1995.

Selroos, J. O., and V. Cvetkovic, Mass flux statistics of kinetically sorbing solute in heterogeneous aquifers: Analytical solution and comparison with simulations, *Water Resour. Res.*, 30, 63-69, 1994.

Selroos, J. O., A. Winberg, and V. Cvetkovic, Design contraints and process discrimination for the detailed scale tracer experiments at Äspö - Multiple well tracer experiment and matrix diffusion, SKB (Swedish Nuclear Fuel and Waste Management Company) International Cooperation Report ICR 94-04, Stockholm, Sweden, 1994.

Tsang, Y. W., Usage of "equivalent apertures" for rock fractures as derived from hydraulic and tracer tests, *Water Resour. Res.*, 28, 1451-1455, 1992.

Winberg, A., Tracer Retention Understanding Experiment (TRUE), Test Plan for the First TRUE Stage, SKB (Swedish Nuclear Fuel and Waste Management Company) Progress Report PR 25-94-35, Stockholm, Sweden, 1994.

List of SKB reports

Annual Reports

1977-78
TR 121
KBS Technical Reports 1 – 120
Summaries
Stockholm, May 1979

1979
TR 79-28
The KBS Annual Report 1979
KBS Technical Reports 79-01 – 79-27
Summaries
Stockholm, March 1980

1980
TR 80-26
The KBS Annual Report 1980
KBS Technical Reports 80-01 – 80-25
Summaries
Stockholm, March 1981

1981
TR 81-17
The KBS Annual Report 1981
KBS Technical Reports 81-01 – 81-16
Summaries
Stockholm, April 1982

1982
TR 82-28
The KBS Annual Report 1982
KBS Technical Reports 82-01 – 82-27
Summaries
Stockholm, July 1983

1983
TR 83-77
The KBS Annual Report 1983
KBS Technical Reports 83-01 – 83-76
Summaries
Stockholm, June 1984

1984
TR 85-01
Annual Research and Development Report 1984
Including Summaries of Technical Reports Issued during 1984. (Technical Reports 84-01 – 84-19)
Stockholm, June 1985

1985
TR 85-20
Annual Research and Development Report 1985
Including Summaries of Technical Reports Issued during 1985. (Technical Reports 85-01 – 85-19)
Stockholm, May 1986

1986
TR 86-31
SKB Annual Report 1986
Including Summaries of Technical Reports Issued during 1986
Stockholm, May 1987

1987
TR 87-33
SKB Annual Report 1987
Including Summaries of Technical Reports Issued during 1987
Stockholm, May 1988

1988
TR 88-32
SKB Annual Report 1988
Including Summaries of Technical Reports Issued during 1988
Stockholm, May 1989

1989
TR 89-40
SKB Annual Report 1989
Including Summaries of Technical Reports Issued during 1989
Stockholm, May 1990

1990
TR 90-46
SKB Annual Report 1990
Including Summaries of Technical Reports Issued during 1990
Stockholm, May 1991

1991
TR 91-64
SKB Annual Report 1991
Including Summaries of Technical Reports Issued during 1991
Stockholm, April 1992

1992
TR 92-46
SKB Annual Report 1992
Including Summaries of Technical Reports Issued during 1992
Stockholm, May 1993

1993
TR 93-34
SKB Annual Report 1993
Including Summaries of Technical Reports Issued during 1993
Stockholm, May 1994

1994

TR 94-33

SKB Annual Report 1994

Including Summaries of Technical Reports Issued during 1994.
Stockholm, May 1995

1995

TR 95-37

SKB Annual Report 1995

Including Summaries of Technical Reports Issued during 1995.
Stockholm, May 1996

List of SKB Technical Reports 1996

TR 96-01

Bacteria, colloids and organic carbon in groundwater at the Bangombé site in the Oklo area

Karsten Pedersen (editor)
Department of General and Marine Microbiology,
The Lundberg Institute, Göteborg University,
Göteborg, Sweden
February 1996

TR 96-02

Microbial analysis of the buffer/container experiment at AECL´s Underground Research Laboratory

S Stroes-Gascoyne[1], K Pedersen[2], S Daumas[3],
C J Hamon[1], S A Haveman[1], T L Delaney[1],
S Ekendahl[2], N Jahromi[2], J Arlinger[2], L Hallbeck[2],
K Dekeyser[3]
[1] AECL, Whiteshell Laboratories, Pinawa, Manitoba, Canada
[2] University of Göteborg, Department of General and Marine Microbiology, Göteborg, Sweden
[3] Guigues Recherche Appliquée en Microbiologie (GRAM), Aix-en-Provence, France
1996

TR 96-03

Reduction of Tc (VII) and Np (V) in solution by ferrous iron. A laboratory study of homogeneous and heterogeneous redox processes

Daqing Cui, Trygve E Eriksen
Department of Chemistry, Nuclear Chemistry,
Royal Institute of Technology, Stockholm, Sweden
March 1996

TR 96-04

Revisiting Poços de Caldas. Application of the co-precipitation approach to establish realistic solubility limits for performance assessment

Jordi Bruno, Lara Duro, Salvador Jordana,
Esther Cera
QuantiSci, Barcelona, Spain
February 1996

TR 96-05

SR 95

Template for safety reports with descriptive example
SKB
December 1995

TR 96-06

Äspö Hard Rock Laboratory Annual Report 1995

SKB
April 1996

TR 96-07

Criticality in a high level waste repository. A review of some important factors and an assessment of the lessons that can be learned from the Oklo reactors

Virginia M Oversby
VMO Konsult
June 1996

TR 96-08

A reappraisal of some Cigar Lake issues of importance to performance assessment

John Smellie[1], Fred Karlsson[2]
[1] Conterra AB
[2] SKB
July 1996

TR 96-09

The long-term stability of cement. Leaching tests

Ingemar Engkvist, Yngve Albinsson,
Wanda Johansson Engkvist
Chalmers University of Technology,
Göteborg, Sweden
June 1996

TR 96-10

Lake-tilting investigations in southern Sweden

Tore Påsse
Sveriges geologiska undersökning,
Göteborg, Sweden
April 1996

TR 96-11
Thermoelastic stress due to an instantaneous finite line heat source in an infinite medium
Johan Claesson, Göran Hellström
Depts. of Building Physics and Mathematical Physics, Lund University, Lund, Sweden
September 1995

TR 96-12
Temperature field due to time-dependent heat sources in a large rectangular grid
– Derivation of analytical solution
Johan Claesson, Thomas Probert
Depts. of Building Physics and Mathematical Physics, Lund University, Lund, Sweden
January 1996

TR 96-13
Thermoelastic stress due to a rectangular heat source in a semi-infinite medium
– Derivation of an analytical solution
Johan Claesson, Thomas Probert
Depts. of Building Physics and Mathematical Physics, Lund University, Lund, Sweden
May 1996

TR 96-14
Oklo: Des reacteurs nucleaires fossiles (Oklo: The fossil nuclear reactors). Physics study (R Naudet, CEA)
– Translation of chapters 6, 13, and conclusions
V O Oversby
VMO Konsult
September 1996

TR 96-15
PLAN 96
Costs for management of the radioactive waste from nuclear power production
Swedish Nuclear Fuel and Waste Management Co
June 1996

TR 96-16
Diffusion of I^-, Cs^+ and Sr^{2+} in compacted bentonite
– Anion exclusion and surface diffusion
Trygve E Eriksen, Mats Jansson
Royal Institute of Technology, Department of Chemistry, Nuclear Chemistry, Stockholm
November 1996

TR 96-17
Hydrophilic actinide complexation studied by solvent extraction radiotracer technique
Jan Rydberg
Department of Nuclear Chemistry, Chalmers University of Technology, Gothenburg, Sweden and Radiochemistry Consultant Group AB, V. Frölunda, Sweden
October 1996

TR 96-18
Information, conservation and retrieval
Torsten Eng[1], Erik Norberg[2], Jarl Torbacke[3], Mikael Jensen[4]
[1] Swedish Nuclear Fuel and Waste Management Co (SKB)
[2] National Swedish Archives
[3] Department of History, Stockholm University
[4] Swedish Radiation Protection Institute (SSI)
December 1996

TR 96-19
Application of space geodetic techniques for the determination of intraplate deformations and movements in relation with the postglacial rebound of Fennoscandia
Hans-Georg Scherneck, Jan M Johansson, Gunnar Elgered
Chalmers University of Technology, Onsala Space Observatory, Onsala, Sweden
April 1996